X-Ray Absorption and Emission Spectroscopy for Catalysis

UNIVERSITÀ DEGLI STUDI DI TORINO

J.A. van Bokhoven, and C. Lamberti

"X-ray absorption and emission spectroscopy for catalysis"

in *X-Ray Absorption and X-ray Emission Spectroscopy: Theory and Applications*, J. A. van Bokhoven and C. Lamberti (Eds), Vol. 2, Chapter 13, John Wiley & Sons, Chichester (UK), 2016, pp. 353-383

doi: 10.1002/9781118844243.ch13

X-ray absorption and emission spectroscopy for catalysis

Jeroen A. van Bokhoven[*,a,b] and Carlo Lamberti[c,d]

[a] *Institute for Chemical and Bioengineering, ETH Zürich, CH-8093 Zurich, Switzerland*

[b] *Swiss Light Source, Paul Scherrer Institute, CH-5232 Villigen PSI, Switzerland*

[c] *Department of Chemistry and NIS, CrisDi Interdepartmental Centers Center of Excellence, Universitàdi Torino and INSTM Reference center, University of Turin Center, Via P. Giuria 7, I-10125 Torino, Italy*

[d] *Southern Federal University, Zorge street 5, 344090 Rostov-on-Don, Russia*

Contact information: j.a.vanbokhoven@chem.ethz.ch

1. Introduction

Catalysis is the enabling technology for production of chemicals and fuels, in the refinery, and in energy conversion [1]. About 80% of all products have been in contact with a catalyst during their manufacture. It is increasingly essential to introduce sustainability and this, together with the change in resource from fossil to durable ones like biomass, requires the development of new catalysts and catalytic processes. The understanding of the fundamental reactions steps that occur on the catalyst surface and their relation to catalyst structure greatly helps the development of new catalytic processes and may suggest a recipe of synthesis new catalysts. Emerging tools that provide control of structure at the molecular level greatly help the development of new catalysts. *In situ* and *operando* characterization of catalysts has significantly contributed to the understanding of how a catalyst functions.

Catalysis is a field that has traditionally benefitted enormously from the application of X-ray absorption and emission spectroscopies (XAS and XES) [2,3]. The often amorphous nature of the catalytically active site and the need to measure under catalytically relevant conditions are the obvious reasons for this. Heterogeneous and homogeneous catalytic systems can be assessed under actual conditions of pressure, sometimes up to hundreds of bars, and temperature (in excess of 1000 °C) [1]. In addition, because a time resolution can be achieved that is the same or comparable to those of catalyst pretreatment and even reaction kinetics, there are increasing possibilities to determine the structure of the ensemble of atoms that form the catalytically active sites [4,5]. Methods emerge that selectively identify the structure of the sites that reacts with reactants and intermediates. Finally, space resolution has enabled measuring catalyst structure as function of position within a single reactor and even of individual catalyst particles [6,7]. This book highlights what is currently possible using many of these methods, some of them providing catalytic examples [8-17]. During the past few years, various authoritative reviews and book chapters about the application of XAS and XES to catalysis have appeared, mostly focusing on heterogeneous catalysis [2-7,18-51] though homogeneous catalysis is also discussed [51-53]. These give an excellent overview of the current state of the art. The aim of this chapter is to provide insight into how XAS and XES can be applied to unravel fundamental questions that relate to the catalytic process. Thus instead of summarizing the literature to date, the focus is on how XAS and XES can help unravel the relation between structure and the essential reaction steps in catalysis. As the large majority of commercial applications and of academic studies

focus on heterogeneous catalysis that is where the emphasis is. Thus, the chapter starts with an introduction into the catalytic process and what are the individual reaction steps that must occur to generate a catalytic cycle. This is followed by a section describing how the measurement condition affects catalyst structure and how the structure of catalytically active sites can be measured. Emphasis is placed on how measuring catalyst structure relates to reaction kinetics. The importance of space and time-resolved measurements is illustrated by selected examples. The chapter ends with a summarizing description of state-of-the-art and an outlook.

2. The catalytic process

A catalyst speeds up a reaction by generating new reaction paths that overall yield a lower activation barrier [1,3]. It does this by breaking bonds and making bonds. Thus, during a catalytic reaction, intermediates are strongly adsorbed, chemisorbed, to the catalyst surface. The formation of a chemical bond, which often has a bond strength in access of a few 100 kJ/mol, may be accompanied by charge transfer and a change in the local structure of the catalytically active site. Figure 1 schematically illustrates the catalytic process. Three events must all occur for a catalyst to be catalytically active. The first is adsorption of the reactant forming a reaction intermediate or intermediates that is or are strongly bonded to the catalyst surface. The figure illustrates associative adsorption of the grey di-atomic molecule and dissociative adsorption of the red one. A typical example of dissociated adsorption is di-hydrogen (H_2) on metals for hydrogenation reactions, one of associative adsorption is CO on metals for CO oxidation. The second event is the surface reaction, in this case the exchange reaction of red and grey atoms. The surface reaction generally consists of multiple steps and may be very complex. A well-known example is the step-wise formation of N-H bonds in the ammonia synthesis [54,55]. Di-nitrogen and di-hydrogen dissociatively adsorb on the surface of the catalyst, for example iron. There is the consecutive addition of hydrogen atoms to nitrogen, until ammonia is formed. All these nitrogen – hydrogen bond formation steps occur at the surface and the catalyst enables these reactions by providing a new reaction path that overall has a lower activation barrier than the non-catalyzed gas-phase reaction. During these reactions, intermediates and product(s) remain (chemi)sorbed to the surface. In the third essential event, desorption of the product(s) occurs, which completes a catalytic cycle. This frees the surface to generate an empty site for new reactants to enter a new catalytic cycle of adsorption, reaction, and desorption. In the figure,

events are drawn as irreversible. In reality, all these processes are reversible. A catalyst catalyzing the reaction of A to B also catalyzes that of B to A. This has to be the case, because the catalyst does not change the thermodynamics of the reaction, it changes the speed at which the equilibrium is reached. That not always the thermodynamic equilibrium is reached is because catalysts selectively enhance reaction paths.

An essential concept in catalysis is the rate-limiting step (RLS), also known as rate-determining step. The rate of the overall process is determined by the slowest step. Often, the RLS is one of the surface reaction steps, however, examples exist where this is not the case and other events are rate determining, like diffusion, adsorption, and desorption. A clear example of this is carbon monoxide oxidation over platinum catalysts under oxygen-lean conditions. The surface of the metal is completely covered by carbon monoxide hindering the adsorption and reaction of di-oxygen. Desorption of a carbon monoxide molecule is needed to free a site for di-oxygen to adsorb and dissociate [56]. Adsorbed oxygen atoms rapidly react to adsorbed carbon monoxide to form carbon dioxide. This simple example shows that to understand the interplay between catalyst, reactant, intermediate and product, the surface reaction mechanism must be understood. Knowledge of the RLS is important when characterizing the catalyst structure. Relative to the RLS, all other reactions are fast and can be assumed to be in equilibrium. For example, in case the surface reaction is the RLS, the adsorption and desorption reactions of reactant are in equilibrium and the surface coverage of reactant intermediates is in equilibrium. Because there is always the forward reaction overall, it is called quasi-equilibrium.

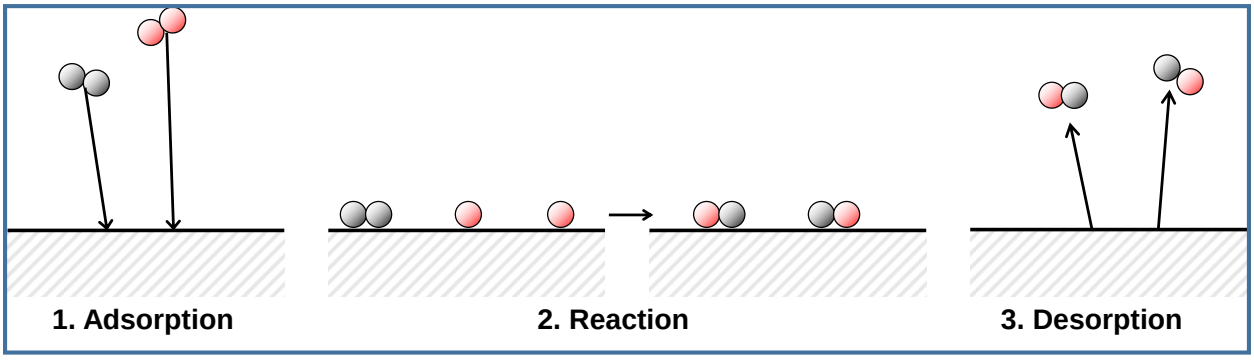

Figure 1. A catalytic reaction consists of three fundamental events. Step 1: adsorption; here associative adsorption of the grey molecule and dissociative adsorption of the red molecule. Step 2: the surface reaction; here the exchange between grey and red atoms. Step 3: desorption of product(s). Together they form the catalytic cycle, which is repeated multiple times during catalytic reaction. Unpublished figure.

The vast majority of *in situ* and *operando* XAS and XES studies focuses on the determination of the structure of the catalyst and that of intermediates and some results in the determination of the RLS [57,58]. Figure 1 directly illustrates why measuring under actual catalytic conditions, or those relevant to it, is so essential. As said, the bond between catalyst and the intermediate is strong and will affect the geometric and electronic structure of the catalyst as described below. However, simply measuring the averaged structure of a functioning catalyst does not necessarily lead to appreciation of the structure of the catalytically active site. The surface of a heterogeneous catalyst is very heterogeneous. For example, a supported metal catalyst consists of nano-sized particles of an active metal attached to a support, which may be inert or exert a catalytic function itself, or directly modify the activity of the particle by affecting the shape of the particle and / or its electronic structure (Figure 2). Also, the particle size is heterogeneous and each particle has many different surface atoms and ensembles of atoms. The quantitative elucidation which of these sites contributes to activity and the definite determination of their structure are extremely difficult. It is one of the aims of this chapter to illustrate the current state-of-the-art in determining the structures of the actual catalytically active sites using XAS and XES.

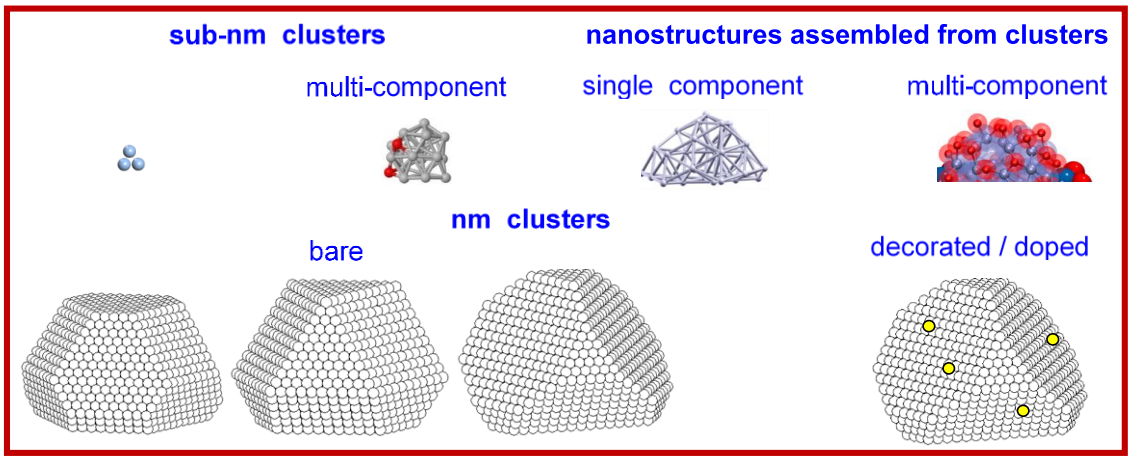

Figure 2. The structure of a heterogeneous catalyst is intrinsically heterogeneous. Single atoms, (sub)nanometer-sized clusters and particles may all be present on the surface of a support, which itself may have multiple surface sites and defects. Courtesy of Prof. Dr. Stefan Vajda.

2.1 From vacuum and single crystals to realistic pressure and relevant samples

As mentioned above, measuring the catalyst structure under actual catalytic conditions is currently in fashion: *in situ* or *operando* spectroscopy [59] is targeting the structure of a functioning catalyst and the aim is to determine structure – performance relations. Much instrumentation development targets at bridging the pressure and materials gaps, thus moving from ultrahigh vacuum and single crystals to realistic conditions, actual catalyst particles, and measuring "real" catalytic reactors. Very regularly new reactor designs are reported in which the catalyst experiences conditions that mimic those in realistic conditions very accurately [2,60]. One can safely say that a single crystal operated in UHV is not a catalyst that produces significant yield of product. However, the more important question is, is what is measured on a single crystal under UHV conditions, relevant to what happens on the surface of a real catalyst under actual catalytic conditions? Much of our understanding of the chemistry at surfaces originates from single crystal work under UHV conditions, because the structure is known to such great detail. The question that we address here is, under what conditions is the structure that is measured under *in situ* and *operando* conditions on a real catalyst within an actual reactor relevant to catalyst performance? The answer to this question depends very much on how the measurement is performed.

There is little doubt that measurements that determine structure under the actual catalytic conditions and on genuine catalysts are the most representative ones. However, this does not automatically mean that the desired structure – performance relation is determined and that the results are unambiguous. The catalytically active sites themselves have the tendency to remain hidden in the majority of species that dominate the spectroscopic signal [61]. Simply flowing reactant gases over a catalyst and simultaneously measuring structure and conversion does not automatically yield the structure – performance relation.

2.2 From chemisorption to conversion and reaction kinetics

Taking the dissociative adsorption of di-hydrogen on the surface of a metal as an example, the influence of reaction conditions on catalyst structure may be illustrated. The hydrogen – hydrogen bond strength is about 420 kJ/mol, which means that to break this bond, the new bonds with the catalyst surface must exceed twice 210 kJ/mol as two new bonds between catalyst and hydrogen atom are formed. This strong chemisorption leads to electronic and geometric structural changes in the cluster that adsorbs the hydrogen bulk atoms [62-66]. Additional

complexity may arise from absorption of atoms into the bulk of the particle or cluster. Palladium is a well-known example that absorbs hydrogen and carbon atoms into the bulk forming sub-surface species or even hydride [67-70] carbide [71-73] species, respectively. It is experimentally and theoretically established that the structure, notably particle shape and local atom environment of, for example, platinum nanoparticles change with increasing hydrogen coverage, thus pressure. Charge transfer between hydrogen atom and the surface metal atoms occurs in addition to lengthening of the metal-metal bond length. (*In situ*) XANES and EXAFS studies have largely contributed to these insights. It is exactly such structural changes that require measuring under catalytically relevant conditions as otherwise the interaction and the resulting structural change is not captured.

Chemisorption of adsorbates (reactants and intermediates) is described by Langmuir isotherms (Figure 3), which assumes that i) all sites are equal, ii) there is no adsorbate – adsorbate interaction, and iii) that the maximum coverage is limited to a monolayer [74,75]. As function of pressure of the gas phase, the coverage on the catalyst surface increases until the maximum coverage (θ), of one is achieved. One is the maximum as the coverage is limited to one monolayer coverage. At higher temperatures, the maximum coverage of one is reached at higher pressure.

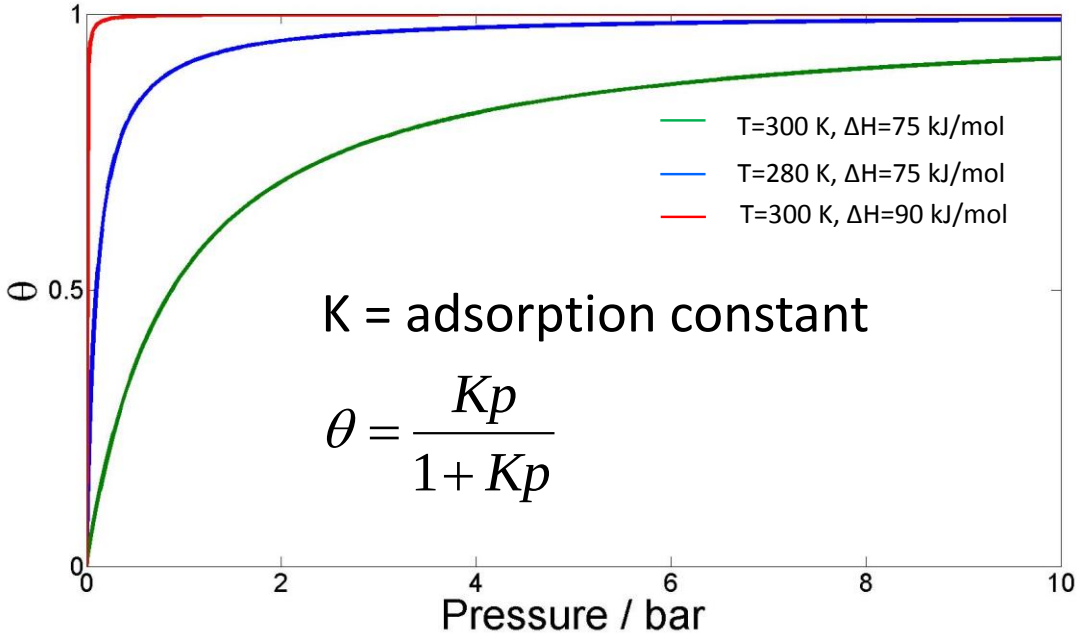

Figure 3. Langmuir isotherms describe the adsorption of species on the catalytic surface. The surface coverage depends on the strength of adsorption via adsorption constant K, the pressure and, temperature. *Operando* and *in situ*

catalytic experiments may be performed under conditions where the surface coverage of one of the reactants and or intermediates is very high or even maximal and all sites are occupied. Unpublished figure.

The amount of adsorbed species is a function of pressure and temperature and thus there is a pressure and temperature dependent catalyst structure. Measuring the same catalyst, with essentially the same structure, thus active sites, in a different (partial) pressure regime or at different temperature, may yield a very different structure, simply because of difference in coverage. Oxygen adsorption on platinum yields chemisorbed oxygen, until at a given pressure the metal oxidizes forming a surface oxide. At even higher oxygen pressure, bulk oxidation occurs. These surfaces have vastly different reactivity [76]. It is important to realize that the partial pressure of a reactant respectively product depends on the conversion level.

It is obvious that in case of high catalytic conversion measuring catalyst structure in a catalytic reactor at different positions may be needed to capture if any change in structure occurs [77,78]. It is the local concentration of gases at the point of measuring, which determines the measured catalyst structure. Because of catalytic conversion, the reducing, respectively oxidizing properties of the gas phase may change to such extend that the structure of the catalyst changes, not only because of the presence of a different coverage of adsorbates, but because a completely different structure forms. The next paragraph gives two notable examples how the structure of a catalyst changes because of changing gas composition of a reacting feed.

2.3 Structural differences within a single catalytic reactor

Catalytic partial oxidation of methane to yield CO and di-hydrogen, syngas, is an important reaction, which eventually produces hydrocarbons via Fischer-Tropsch synthesis, di-hydrogen via the water-gas shift reaction, and methanol via CO hydrogenation. This oxidation reaction is characterized by a light-off behavior or ignition of the reaction. Under specific conditions, a sudden, large increase in catalyst reactivity occurs, which changes the product distribution towards syngas. Typical catalysts are nano-sized nobel metal particles on a support. Coupling a space-resolved CCD-camera with microscopic optics and using a 1.0 mm by 0.6 mm X-ray beam completely irradiating the catalyst within a capillary catalytic reactor (Figure 4, top) enabled determining the catalyst structure as function of position within the reactor. Thus, micrometer-range spatial resolution was achieved, the resolution determined by the detector. The catalytic

rhodium and or platinum particles on an alumina support showed tremendous structural differences within the reactor (Figure 4, bottom) [77]. Below ignition temperature, the catalyst typically only produced CO_2 and water and the metal remained oxidized over the whole catalyst bed [79].

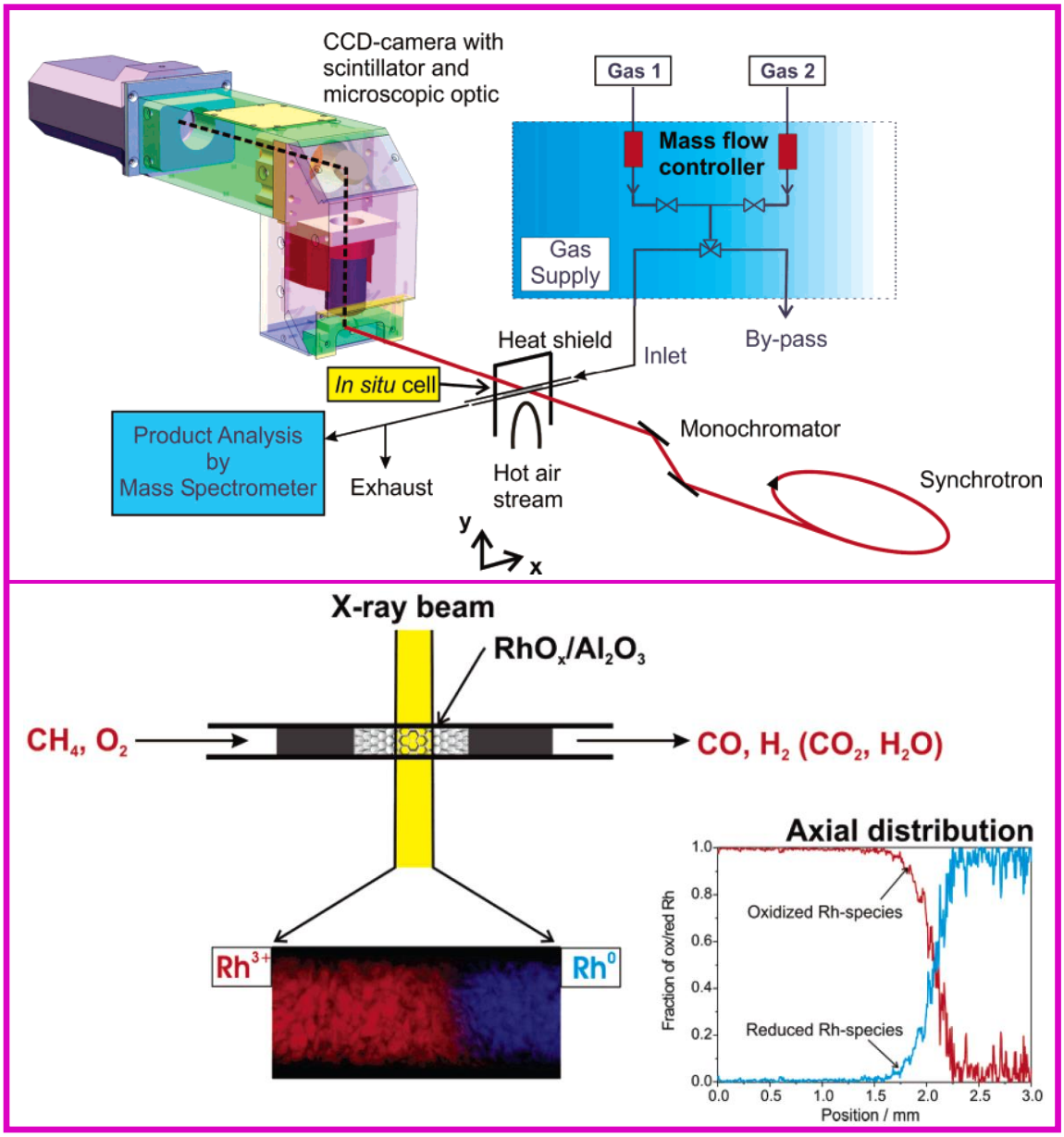

Figure 4. Top: Instrumental setup to measure the structure of a catalyst space-resolved over a catalytic reactor, using a space-resolved detector and a large X-ray beam. On-line mass spectrometry determines the real-time catalyst performance. Bottom: structural variation of a Rh/Al_2O_3 catalyst within a single reactor: initially, the oxidizing conditions result in a cationic state of rhodium. Because of conversion, the environment becomes more reducing,

which causes a zero valence state of rhodium. Inset: axial distribution of catalyst structure. Figure Adapted with permission from ref. [77], copyright ACS, 2006.

However, this situation dramatically changed above the point of ignition, and oxidic and reduced metal (in this case rhodium) were both observed: In the first part of the reactor, there was Rh^{3+}, in the latter part Rh^0 (Figure 4, bottom). The structural changes were within a gradient of less than 100 μm. Measuring space- and time-resolved yields movies that illustrate that reduction started at the end of the reactor bed and progressed towards the inlet of the reactor (See supporting information of refs. [77,78]). Individual catalyst grains tended to reduce from the inside out. Thus at the center of these particles, the conditions were most reducing, which then auto-catalytically accelerated catalyst reduction towards the outer part of the particles.

The second example that illustrates the need to measure catalyst structure as function of exact reaction conditions and position within a single reactor is that of CO oxidation. CO oxidation is a seemingly simple reaction, however, depending on the reaction conditions, the catalyst structure varies widely. All these structures have vastly different catalytic reactivity. One peculiar characteristic of this reaction is that under certain conditions, oscillations may occur. During oscillations, the catalytic reactivity changes periodically [55]. CO oxidation over noble metals occurs in different regimes. Under oxygen lean conditions, CO covers the metal surface and the RLS is CO desorption (vide supra Section 2), after which di-oxygen can dissociatively adsorb and react to form CO_2. Under oxygen-rich conditions, when the reactivity of the catalyst is much higher, in situ XANES and EXAFS at the Pt L_3 edge has identified the presence of a defective and structurally disordered surface oxide [80,81]. *In situ* XAS at the Pt L_3 on Pt/Al_2O_3 during oscillating CO oxidation conditions identified time- and space-resolved structural changes in structure of the platinum nano-particles. Figure 5 shows the mass spectrometer signal that was recorded at the end of the reactor during slowly cooling of the reactor while flowing CO and di-oxygen. Oscillations occurred. Using the quick-scanning mode [9,82] at the Pt L_3 edge it was possible to identify structural changes that occurred at the exact frequency of the oscillations. Initially, high whiteline intensity was observed, and during periods of lower activity, the whiteline intensity decreased proportionally, its intensity following the reactivity of the catalyst indicated by the amount of CO_2 observed at the exhaust of the catalyst. Spectral analysis showed that the structure changed from a platinum particle covered with a surface oxide to that of a CO

covered surface, with the possible presence of an intermediate during re-oxidation. In parallel to oscillations in the activity of the catalyst, identified by the amount of CO_2 at the reactor exhaust, the relative percentage of CO-poisoned surface and surface oxide changed. The amount of the more reactive surface oxide was higher with higher conversion levels.

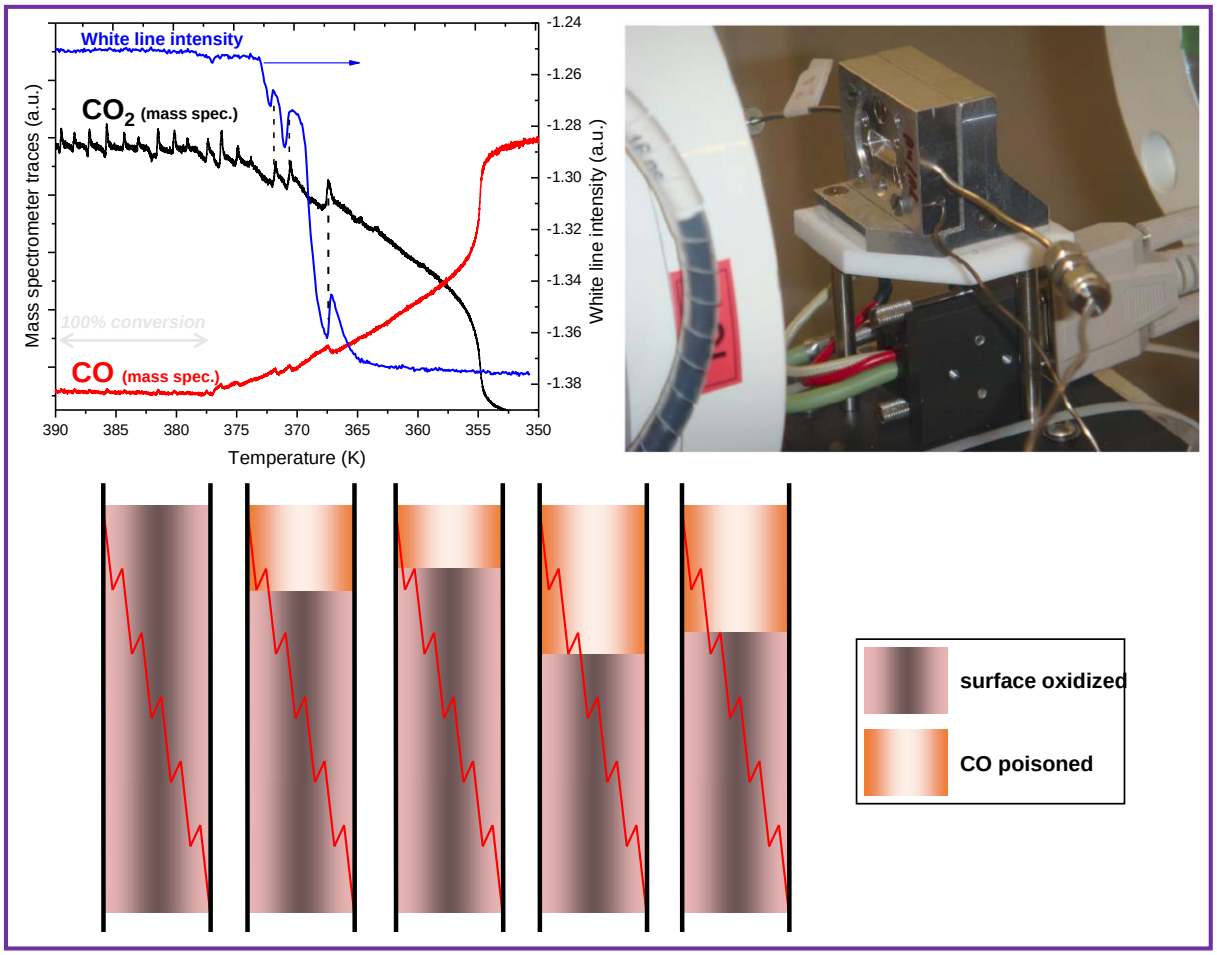

Figure 5. Top left: Mass spectrometer signal recorded at the exhaust of the reactor filled with Pt/Al_2O_3 catalyst during reaction of CO with di-oxygen. Oscillatory behavior is observed especially in the CO_2 signal. The maximum of the whiteline intensity of Pt L_3 edge spectra recorded using a quick-scanning monochromator oscillated in concert with the overall reactivity of the reactor. Repeated measurements at various positions of the catalytic reactor, shown top left, identified that the relative percentages of CO-poisoned surface and surface oxide varied: the border between the top moving from top to bottom of the reactor in an oscillatory fashion. Part of this is shown at the bottom. Figure reproduced with permission from ref. [78], copyright Wiley-VCH, 2010.

In Figure 5, top left, the whiteline intensity initially did not vary with the CO_2 signal. The reason was that although structural changes occurred to the catalyst, they were not captured by the XAS measurement, because the X-ray spot hit the catalyst at a different position of the reactor. The mass spectrometer determines integral performance of the catalyst, the XAS measures only a fraction of the catalyst within a given point of the reactor. Impinging the X-ray spot at a different position of the catalyst bed, showed changes in the whiteline at different levels of conversion: at the highest conversion levels, changes occurred at the top of the catalyst bed, at lower conversion levels, the structural changes took place further down the bed. Thus, the relative amounts of CO-poisoned surface and surface oxide vary with reactivity and the border between them moves from top to bottom of the reactor in an oscillatory manner, part of which is shown in Figure 5, bottom.

Most often, the gas concentration is determined at the exhaust of the reactor. One can also measure the integral catalyst structure [83], which will yield the sum of all structures that are present, which may have some advantages in certain cases. The problem of changing conditions because of conversion over the catalyst is well known in reaction kinetics, where reaction rates and orders are measured under differential condition. The feed contains a controlled amount of reactants and products (and possibly intermediates) and the conditions are chosen, such that there is negligible, or at least very low, conversion per pass over the catalyst bed [84]. Thus the complete catalyst experiences the same environment and equilibrates into a single species. Any measured structure under such conditions can be directly related to performance as determined from the composition at the end of the reactor. Measuring space resolved is not needed in this case. *In situ* and *operando* characterization and kinetic analysis are ideally performed in parallel or at least both taken into account. However, as the examples reported in Figure 4 and Figure 5 show, that to appreciate catalyst structure and performance, the relevant conditions must be chosen and to capture all possible structures, multiple experiments must be performed with different feeds that mimic reactive conditions that are representative of all conditions and conversion levels. Conditions under which 100% conversion is reached must be avoided. At point of measuring, the catalyst may not be converting, but be should be exposed to the reaction products. Ideally, catalyst structure and gas composition is known at all times and all locations within the catalytic reactor. Such experiment has not yet been established in X-ray spectroscopy.

2.4 Determining the structure of the active site

Even if one succeeds in measuring the catalyst structure under precisely known conditions, space and time-resolved, the structure of the active site is still not necessarily uncovered. The number of atoms that form the active site may be only a minor fraction of the total number of atoms (cf. Figure 2). Methods that characterize the bulk or the surface in a non-selective manner may miss the actual reactive species even in *in situ* and *operando* experiments. Single-site catalysts, such as (heterogenized) homogeneous catalysts [85-92] and catalytically active atoms homogeneously distributed in a matrix, for example aluminum or iron atoms in the framework of zeolites [93-97], do not have this limitation. The structures of hetero-atoms in the framework of zeolites as determined by XAS have recently been reviewed [50].

Measuring in the time domain in the kinetically relevant regime may provide a possible solution to the existence of multiple (in)active species. Transient measurements yield the changing structure of catalyst and / or reactant and adsorbate after disturbing the system, such as changing gas composition or isotope composition (as can be detected by infra-red spectroscopy and mass spectrometry). The catalytically active site will rapidly respond to the change in case the disturbance affects a kinetically relevant step. Inactive spectator species may respond, but at a very different, generally much lower, rate [98]. An illustrative transient experiment is that of propylene epoxidation [99]. Using transient Ti K-edge XANES experiments, in which reactant propylene was suddenly removed from the feed, the structural change of the titanium site was detected in a time-resolved manner. A quantitative relation between the rates of steady-state reaction of propylene epoxidation and that of disappearing of the Ti-hydroperoxo species in response to the switch in conditions, identified this species as the reactive intermediate. The existence of a quantitative relation between the rate of a catalytic reaction and that of a transient signal can thus be exploited to unravel the structure of the catalytically active site even in case the catalytically active site is the minority specie. Besides knowledge of the mechanism [75], a fundamental requirement of a successful experiment is the existence of the intermediate at the surface in measurable amounts. This corresponds to all pressures in the Langmuir isotherm, except for the lowest ones (Figure 3) where coverage is close to zero.

Modulation excitation and phase sensitive detection, widely used in IR spectroscopy [100-106], have been recently introduced into the field of X-ray diffraction [107,108] and X-ray absorption spectroscopy [109-114] and in combined EDEXAFS/IR experiments [115]. A clear example is

given in chapter 7 of this book by Nachtegaal, et al. [9] and not repeated here to the same detail. In short, signals that come from minority species that show a selective response to an external impulse or transient, such as change in concentration of reactants, can be detected with very high accuracy, because the signal is selectively isolated and can be fitted assuming the signal is a difference spectrum [110]. Another method to identify intermediate species is multivariate curve resolution (MCR) [116-118]. In MCR a set of time-resolved X-ray absorption spectra are deconvoluted into a number of basic spectra, which make up the total. The concentration profile of all basic spectra can be determined. In contrast to phase sensitive detection, the MCR analysis directly yields the time evolution of the different species in the sample. Thus, time resolution and kinetics of structural changes of minority species are becoming accessible. The few papers that have appeared illustrate the promise of these methods and it is relatively safe to predict that further development and application of these methods will be used to unravel the structure of catalytically active species, even if, or exactly when, these are the minority species.

3. Reaction kinetics from time-resolved XAS

3.1 Oxygen storage materials

Ceria (CeO_2) and cerium-based materials can store oxygen under oxygen-rich conditions and release it under oxygen-deficient conditions. Owing to this oxygen storage/release capacity (OSC), they are widely used as promoters of automobile three-way catalysts and find more and more applications as reaction booster in oxidation and hydrogenation reactions [119-123]. Upon oxygen release and uptake, the cerium oxidation state varies; release of each oxygen atom from ceria yields two Ce^{3+} atoms and one vacancy. Thus, the cerium oxidation state is a function of the reducibility of the feed; switching from oxygen-rich to oxygen-lean feed, something that often occurs in the automotive exhaust, leads to release of oxygen atoms of the support and oxidation reactions will continue, hence the name oxygen storage material. Addition of zirconium cations to ceria dramatically improves the OSC and thermal stability [124]. The most efficient CeO_2–ZrO_2 material is a ceria-zirconia solid solution which has an atomically homogeneous, ordered arrangement of cerium and zirconium ions assigned to the κ-$Ce_2Zr_2O_8$ fluorite phase. The platinum-promoted κ-$Ce_2Zr_2O_8$ transforms into pyrochlore $Ce_2Zr_2O_7$ under the reducing conditions in the working state. Even though the system had been studied by many methods and under varied conditions, no real-time dynamics had been reported. Yamamoto et al.

applied energy dispersive (ED) XANES at the Ce L_3 edge and ED XANES and EXAFS at the Zr K edge to determine the dynamics of the OSC process under actual conditions [125]. The aim was to determine the dynamical changes at both the cerium and zirconium sites upon reducing, thus oxygen release, respectively oxidizing, thus oxygen uptake, conditions. Both zirconium and cerium in κ-$Ce_2Zr_2O_8$ have valence +4 and are eight coordinate. In pyrochlore $Ce_2Zr_2O_7$, the formed specie during oxygen release, cerium (zirconium) atoms have valence +3 (+4) and are eight (six) coordinate.

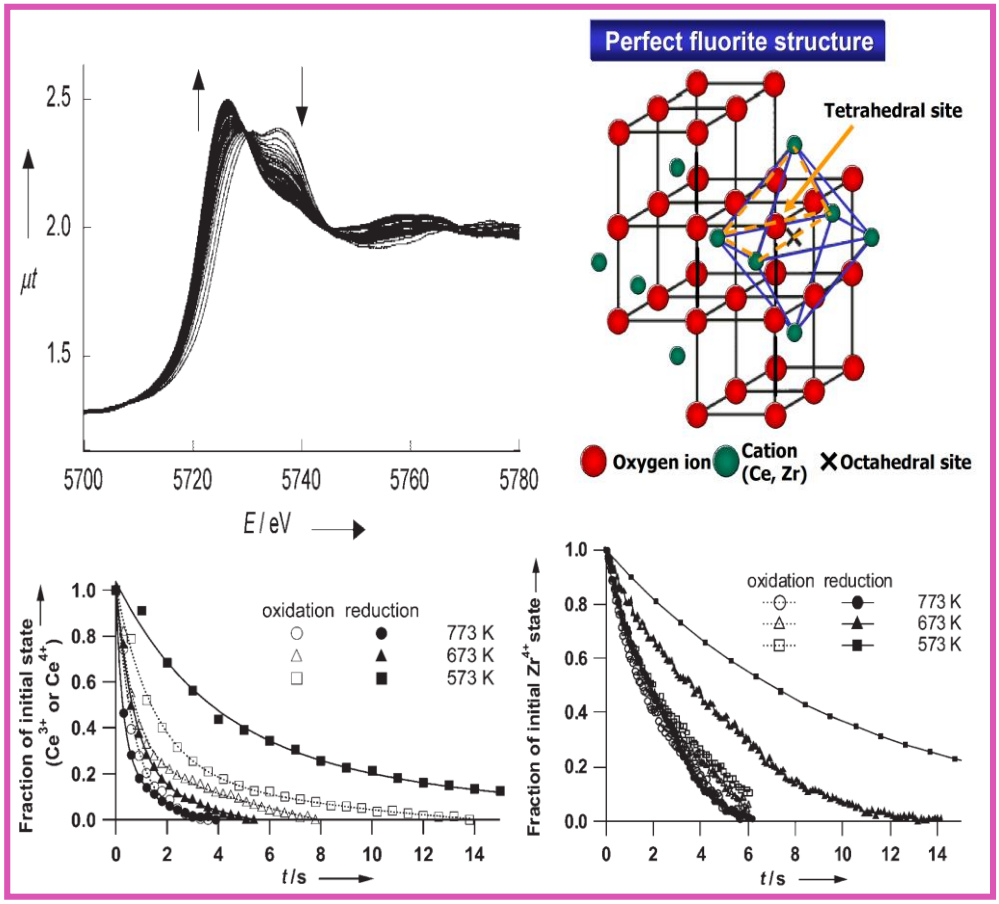

Figure 6. Top-left: Time resolved Ce L_3 edge XANES, recorded by energy-dispersive XAS, during oxygen release of Pt/$Ce_2Zr_2O_8$ at 573 K. Bottom-left: Time-dependence of Ce^{4+} and Ce^{3+} fractions at 573, 673, respectively 773 K during oxidation (open markers) and reduction (closed markers) obtained from Ce L_3 edge data. Bottom-right: Time profiles of the fractions of $Ce_2Zr_2O_7$ and $Ce_2Zr_2O_8$ during the oxygen-storage and -release processes of Pt/$CeZrO_x$ obtained from Zr K-edge data. Top-right: Fluorite structure of $Ce_2Zr_2O_8$ identifying the tetrahedral and octahedral sites. Figure adapted with permission from Ref. [125], copyright Wiley-VCH, 2007.

Figure 6 shows time-resolved Ce L_3-edge ED XANES spectra of Pt/$Ce_2Zr_2O_8$ during oxygen-release at 573 K under 12.4 kPa H_2. The virgin Pt/$Ce_2Zr_2O_8$ sample gives typical Ce L_3 edge doublet white lines characteristic of Ce^{4+} species in $Ce_2Zr_2O_8$ and CeO_2 [126]. Switching to reducing conditions by dosing the di-hydrogen, the doublet transformed into a singlet and the edge position shifted to lower energy, and after 20 s the spectrum became identical to a typical spectrum of Ce^{3+} species in $Ce_2Zr_2O_7$.

The serial Ce L_3 XANES spectra exhibited an isosbestic point, except for the first 0.9 s and the last 2 s of the transformation, which indicates that the majority of κ-$Ce_2Zr_2O_8$ transforms directly into pyrochlore $Ce_2Zr_2O_7$. Exposure to 12.4 kPa oxygen at 573 K, resulted in recovery of the initial doublet feature in the spectrum, indicative of reversibility. Linear combination using reference Ce^{3+} and Ce^{4+} spectra yielded the time-resolved fraction of Ce^{3+}, respectively Ce^{4+} during the reduction, respectively oxidation cycle at three different temperatures (Figure 6, bottom-left). Table 1 shows that a larger temperature-dependence for reduction was observed resulting in activation energy of oxygen storage (release) of 20 (43) kJ/mol. Initial rate constants at 773 K were 1.4 (2.2) s^{-1} for oxygen storage (release).

Table 1. Activation energy and rate constant in oxidation and reduction cycles of Pt/ceria-zirconia between 573 and 773 K as measured at the Ce L_3 edge respectively Zr K edge. Table adapted with permission from Ref. [125], copyright Wiley-VCH, 2007.

	Activation energy (kJ/mol)		Rate constant at 773 K (s^{-1})	
	Oxygen storage	Oxygen release	Oxygen storage	Oxygen release
Measured at Ce site	20	43	1.4	2.2
Measured at Zn site	4	43	0.46	0.39

ED XAS at the complementary Zr K edge yielded the time-resolved changes at the zirconium sites (Figure 6 bottom-right). Full EXAFS analysis, which indicated the same time dependence as the XANES, was provided [125], but not discussed here. Table 1 shows that again a much larger temperature-dependence for reduction was observed resulting in activation energy of oxygen storage (release) of 4 (43) kJ/mol. Initial rate constants at 773 K were 0.46 (0.39) s^{-1} for oxygen storage (release). Remarkably, the electronic and structural transformations at cerium and zirconium sites during the oxygen storage/release processes are not synchronized with each

other in the solid solution. In both the oxygen-storage and –release processes, the valence at the cerium sites changes first, and then structural transformation occurs at the zirconium sites, making respectively breaking of Zr – O bonds. The dynamics at zirconium sites observed by ED XAFS involve changes in local structure and number of coordinated oxygen atoms, as well as oxygen diffusion. This study nicely illustrates how time-resolved XAS data can be used to extract kinetic parameters in an element-specific manner.

3.2 Selective propene oxidation over α-MoO_3

Another clear example, which illustrates the added value of measuring the dynamic nature of surface and bulk structure compared to determining the structure under steady-state reaction conditions is that of oxidation catalyst molybdenum tri-oxide [127-129]. X-ray-based methods are attractive, because during oxidation reactions, the activation of oxygen and the oxidation of the reactant often lead to oxidation and reduction of the catalyst, if only temporarily (cf. Figure 1), which yield different structure and oxidation states and thus clear spectral differences. The selective oxidation of alkenes is commercially applied and is often catalyzed by molybdenum-based catalysts [130]. Using gas-phase oxygen, the Mars-van-Krevelen mechanism is commonly assumed [131]. Oxygen atoms of the catalyst surface and / or bulk react to an adsorbed intermediate to form the desired product leaving the catalyst in a reduced state. Oxygen from the gas phase re-oxidizes the catalyst. In case of propene, the reaction intermediate is assumed to be an allylic species [132], which reacts selectively to acrolein or unselectively to carbon dioxide, which obviously is the undesired product. The resulting oxygen vacancies are replenished by oxygen from the gas phase. The complexity of this mechanism illustrates that time-averaged catalyst structure without knowledge on the time-dependencies of electronic and geometric structure on changing gas phase redox potential provides –at best- only partial insight into the structure–activity correlation.

Propene is oxidized in the presence of oxygen at temperatures above 600 K by α-MoO_3. The averaged valence of molybdenum is somewhat reduced during reaction, because of the different rates of reduction and re-oxidation [133]. Figure 7 shows the in situ time-resolved Mo K-edge spectra of MoO_3 reduction in propene and MoO_2 oxidation in oxygen. Using mass spectrometry, the composition at the reactor exhaust was simultaneously determined. Propene completely reduces MoO_3 to MoO_2, which under oxygen is more rapidly re-oxidized to MoO_3.

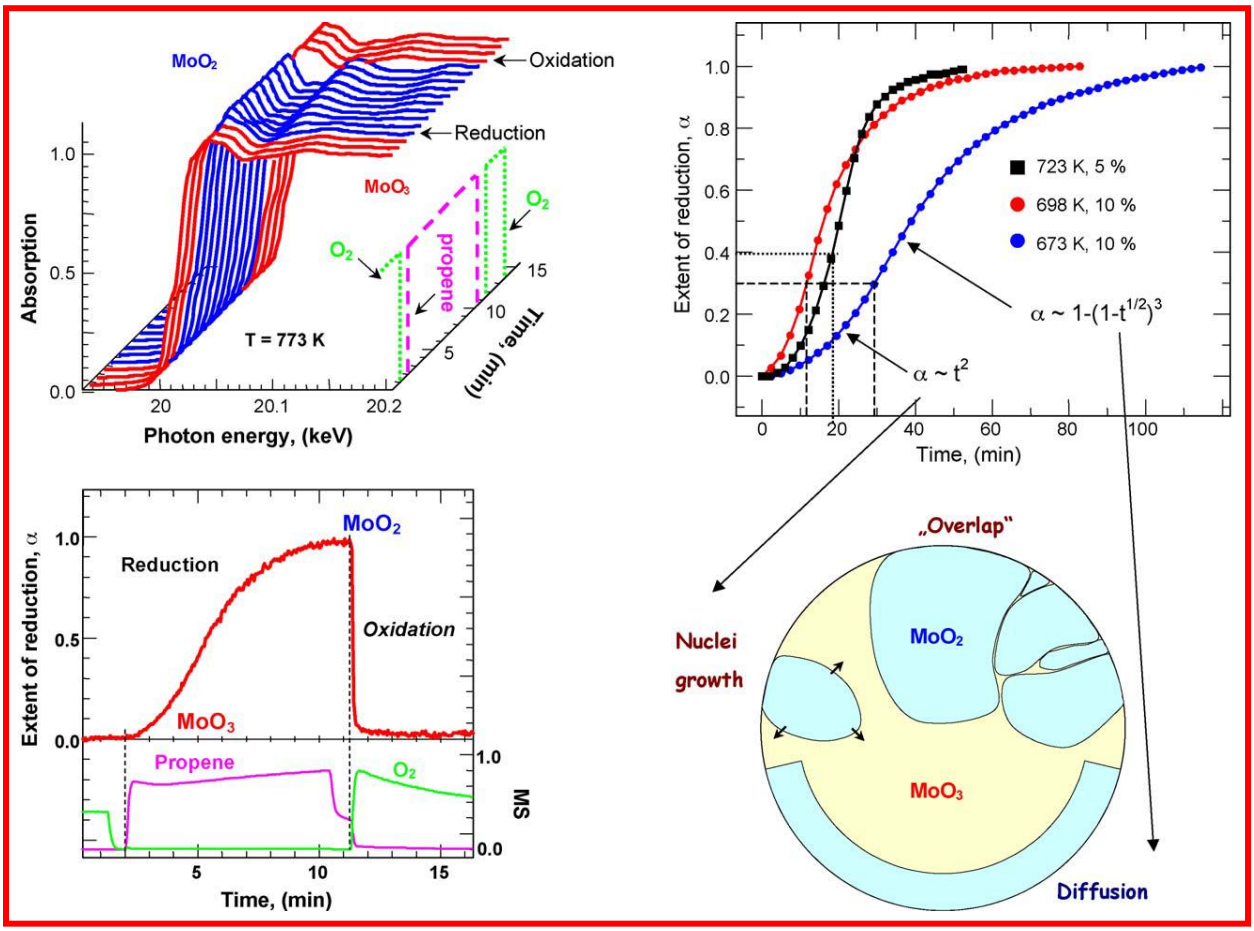

Figure 7. Left side shows spectral changes upon changing the gas environment from oxidizing to reducing and back to oxidizing again. Right side the extent of reduction (a) during isothermal reduction of MoO_3 in 5 vol.% propene at 723 K, and in 10 vol.% propene at 673 K respectively 698 K. A power rate law, ($\alpha \sim t^2$), described the acceleratory regime of the reduction at 673 K (up to $\alpha \sim 0.3$) and a ''three dimensional diffusion'' rate law ($\alpha \sim 1 - (1 - t^{1/2})^3$) the deceleratory regime of the reduction. The solid-state reduction kinetics showed a change in the rate-limiting step, both as with temperature and extent of reduction α. At a given temperature, the nuclei growth kinetics changes to a three dimensional diffusion controlled regime. With decreasing temperature (< 650 K) a transition from nuclei growth kinetics to oxygen-controlled diffusion in the MoO_3 lattice occurred. Figure adapted with permission from ref. [129], copyright Elsevier, 2009.

The following schematic mechanism for reduction of MoO_3 in propene was proposed: (i) propene reaction with oxygen yields vacancies at the (1 0 0) or (0 0 1) facets; (ii) vacancy diffusion in the MoO_3 bulk; (iii) formation of ''$Mo_{18}O_{52}$'' type shear-structures in the lattice; and (iv) formation and growth of MoO_2 nuclei. The re-oxidation of MoO_2 in oxygen proceeds in the

reverse direction from step (iv) to (i). Complete oxidation to MoO_3 only occurred above 720 K [128]. The relation between reduction and oxidation properties with catalytic performance was determined by time-resolved in situ XAS under propene oxidation conditions (273 K to 773 K, and propene to oxygen ratios from 1:1 to 1:5). Reaction between propene and oxygen commenced with the onset of the reduction of MoO_3. At lower temperatures, formation of ''$Mo_{18}O_{52}$'' type defects in the layered structure of α-MoO_3 was observed. At temperatures above 720 K and in strongly oxidizing atmosphere, the ''$Mo_{18}O_{52}$'' type defects re-oxidized. These data enabled making conclusions about the evolution of three stages of structural evolution of MoO_3 under selective oxidation conditions (Figure 8): (i) Below ~ 600 K, no selective oxidation occurs and oxygen from the MoO_3 bulk does not participate; (ii) between ~ 600 K and ~ 700 K oxygen vacancy diffusion in the bulk enables the redox mechanism forming the ''$Mo_{18}O_{52}$'' type shear-structures is inhibited, which is thus the phase detected under reaction conditions; (iii) Above ~ 700 K sufficiently fast oxygen diffusion in the lattice permits the participation of a considerable amount of the lattice oxygen of MoO_3 in the partial oxidation of propene. The reduced average molybdenum valence of MoO_3 under reaction conditions at temperature below ~ 700 K correlates with the inferior selectivity of the material [134].

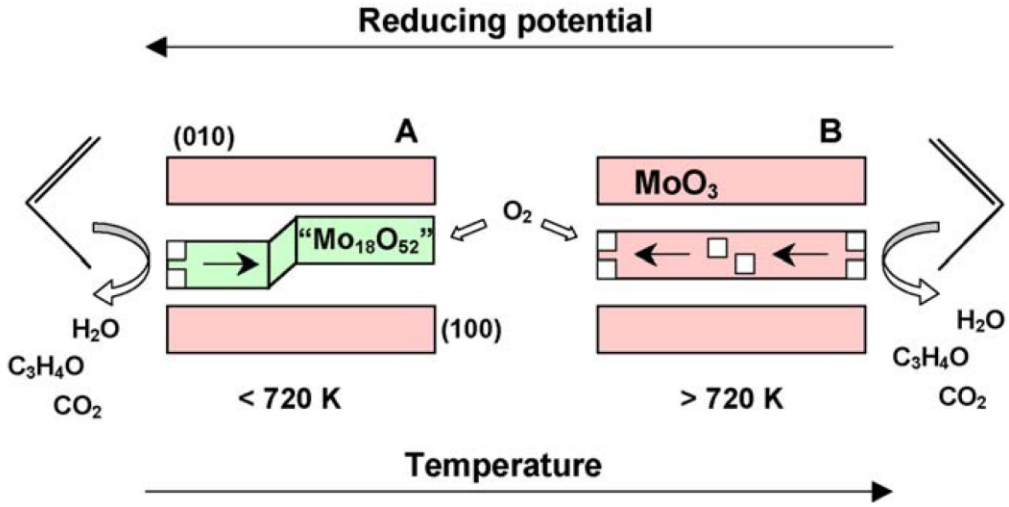

Figure 8. Structural changes in MoO_3 under propene oxidation conditions as function of temperature and gas environment. A. Below 720 K and in reducing environment, reduction occurs and $Mo_{18}O_{52}$ shear-type defects in the MoO_3 structure form; B. Above 720 K and in oxidizing environment MoO_3 with few oxygen vacancies (squares) form. Figure adapted with permission from ref. [129], copyright Elsevier, 2009.

3.3 Active sites of the dream reaction, the direct conversion of benzene to phenol

Phenol is a base chemical and the source for many resins. It is produced by the well-known three-step cumene process via a hydroperoxide species [135]. This process produces stoichiometric amounts of acetone as side-product. Replacing this multi-step process by a one-step direct synthesis from benzene, and without the formation of stoichiometric side products, remains one of the most desirable catalytic reactions. Partial oxidation, however, is hampered by side reactions, mainly over-oxidation to carbon dioxide. Many oxidizing agents are being investigated, however, using di-oxygen as oxidant is highly desirable. Invariably, high selectivity can only be achieved at low benzene conversion and high conversion leads to decreased selectivity.

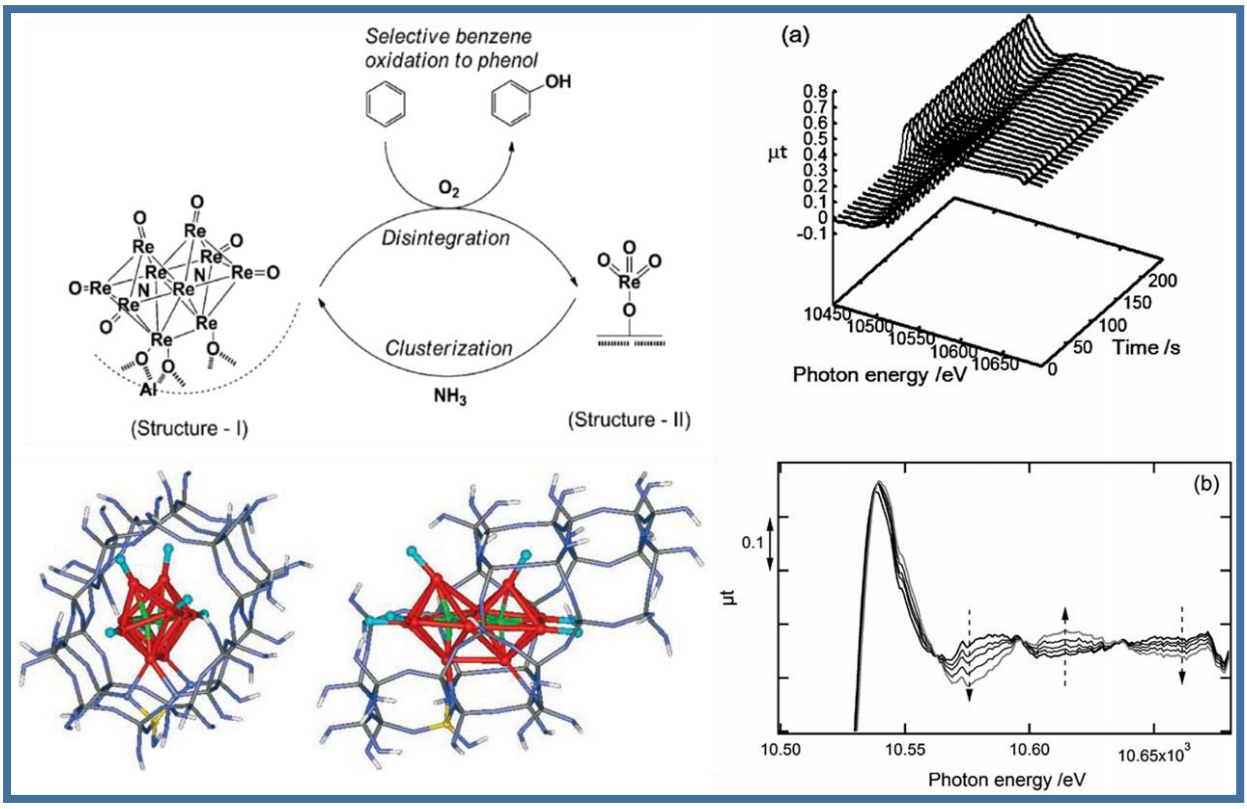

Figure 9. Top left: Formation and disintegration of the active Re_{10} cluster for selective benzene to phenol conversion; Bottom left: Re_{10} cluster depicted in the pores of the zeolite. Right side: in situ L_3 edge Re dispersive XANES during structural transformation between structure I and structure II showing isobestic points, bottom left. Figure adapted with permission from Ref. [136], copyright Wiley-VCH, 2006.

Recent developments yielded [136] a rhenium catalyst supported on H-ZSM-5, which achieves phenol selectivity of 93.9% at 9.9% conversion in a pulse reactor and 87.7% at 5.8% conversion under steady-state conditions and in the presence of NH_3. Through time-resolved X-ray spectroscopy at the Re L_3 and L_1 edges using energy dispersive XAS and step-scan XAFS, dynamic changes of catalyst structure were observed. XAFS fitting and XPS identified that the catalyst structure dynamically changed between a monomeric and multimeric structure (Figure 9). Ammonia treatment of the synthesized catalyst yielded a Re_{10} cluster incorporating two nitrogen atoms. Phenol production by exposure to benzene and di-oxygen caused the Re_{10} clusters to decompose and form rhenium monomers. The surface sensitivity of XPS identified that the Re_{10} cluster was located at or close to the external zeolite surface, whereas the monomers were dispersed throughout the zeolite pores. These monomers were inactive.

The difference in rhenium oxidation state could be observed in the L_3 edge whiteline: the Re^{7+} monomer exhibiting higher intensity than the $Re^{3/4+}$ clusters. Time-resolved measuring enabled to determine the transformation of the two species. The spectra showed isobestic points indicating that the Re_{10} cluster (Figure 9, structure I) directly converts into the rhenium monomer (Figure 9, structure II) without any metastable intermediate at the measured time scale. At all stages, the measured spectra could be satisfactorily represented by a linear combination of the initial and final state spectra following:

$$\mu t(t) = P(t)\mu t_i + Q(t)\mu t_f \qquad (1)$$

where μt_i and μt_f represent μt of the initial state, which is the Re_{10} cluster and the final state the rhenium monomer, respectively. P(t) and Q(t) are coefficient parameters that represent the amounts of both structures. The sum of the coefficients P(t) and Q(t) was always 1.0 ± 0.005 at all stages of the oxidation process, showing the absence of (measurable) intermediates. Rate constants of the Re_{10}-cluster disintegration were estimated by the kinetics of the estimated P(t) [137]. Rate constants (k) of the Re_{10}-cluster disintegration were described by:

$$\begin{aligned} -d[\text{structure I}]/dt &= k\, pO_2^{\alpha}\, [\text{structure I}] \qquad (2)\\ &= k'[\text{structure I}] \\ k' &= kpO_2^{\alpha} \end{aligned}$$

[structure I] is replaced by the coefficient of structure I, P(t), enabling determining the reaction order in di-oxygen, α using:

$$ln\, k' = ln\, k + \alpha\, ln\, pO_2 \qquad (3)$$

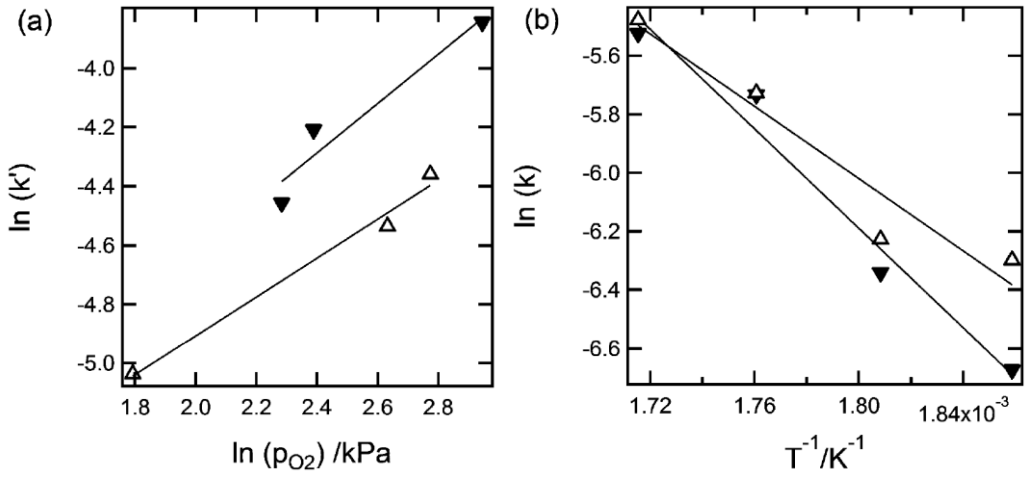

Figure 10. (a) Reaction order of oxygen pressure (pO_2) for the Re_{10}-cluster disintegration from structure I to structure II at 553 K. (b) Arrhenius plots for the Re_{10}-cluster disintegration from structure I to structure II. Open triangles: reaction with oxygen in the absence of benzene and closed triangles: reaction with oxygen and benzene (pressure benzene = 4.8 kPa). Figure reproduced with permission from Ref. [137], copyright RSC, 2010.

Figure 10a shows the relationship between ln k′ and ln pO_2 in the absence (open triangles) respectively presence (open triangles) of benzene. The following orders in oxygen were observed: Linear fittings yielded an order equal to 0.65 in the case of oxygen only and to 0.83 in the case of the mixture of oxygen and benzene. The latter value correlates to the first order of di-oxygen for the phenol synthesis. Oxygen dissociates on the Re_{10} cluster. One of the oxygen atoms attacks a C–H bond of a coordinated benzene molecule followed by insertion into the C–H bond. Oxygen dissociation is paralleled by removal of an interstitial N atom from the rhenium cluster, destabilizing it. The second oxygen atom does not react to benzene, but is consumed for the disintegration of the Re_{10} cluster. This yields the first order oxygen dependence of phenol formation. Using k′ and α, at four reaction temperatures yielded the activation energy (E_{act}) of the Re_{10}-cluster disintegration (Figure 10b). E_{act} in the absence of benzene was 51 ± 7 kJ mol/1,

while in the presence of benzene it was 71 ± 7 kJ mol/1. This indicates that benzene inhibits the disintegration of the catalytically active Re_{10} cluster. The absence of metastable intermediate structures may be advantageous for achieving high phenol selectivity. The competition between disintegration and formation of the Re_{10} cluster and their relative rate was identified by the averaged structure of the catalyst under reaction conditions: an estimated 5% was in the form of active rhenium clusters [136,138].

As was the case for propene oxidation over MoO_3, the catalyst structure under reaction conditions was unique and differed from the starting compound. The time-resolved measurements enabled identifying the origin of these averaged structures, illuminating details about the reaction mechanism and identifying relevant catalytic species. The relative rates of oxidation vs. reduction and cluster formation vs. disintegration affect the average structure of the catalyst. Measuring under catalytic relevant conditions, like in situ and operando, is essential; adding time resolution enables identifying the actual active compounds and yield the understanding needed to appreciate catalytic performance. The examples illustrate that kinetics using spectroscopy has become possible and yields insight into the structural modifications that occur during individual reaction steps.

4 Sub-micrometer space resolved measurements

Measuring structure dependence of a catalyst within a catalytic reactor has been addressed above (Figure 4 and Figure 5). The EXAFS analysis yields the local structure at various positions within a reactor and even within a single catalyst grain. However, there is a large interest towards measuring structure space-resolved at all length scales that are of interest to catalysis: The dimensions of a catalytically active site is in the order of Ångstrøm. Often these are associated with nano-sized particles that are attached to a support. The size of support particles is in the order of tens or hundreds of nano-meter. However, because packing such very small particles into a reactor leads to plugging of the reactor, they are formulated into shaped particles, the size of which is in the millimeter and centimeter range. Industry has perfected the art of making such particles. Of utmost importance is the distribution of active sites and for reactants and products to diffuse to respectively from these sites through the pores of the formulated catalysts. Formulations with micro-, meso-, and macro-pores are engineered to achieve this goal. Micro-pores are defined as having a diameter below two nm; meso-pores between two and 50 nm, and

macro-pores lager than 50 nm. Structural characterization at all these length scales is essential to appreciate the functioning of the catalyst and there is much effort to characterize catalysts at the sub-micrometer length scale [139]. Naturally, measurements are to be executed under relevant, in situ conditions if relevant catalytic structures are sought. Chapter 10 of this book [140] illustrates the possibility and limitations of using (sub)micrometer sized beams to measure structure. Other methods include the scanning transmission X-ray microscope (STXM), the photo-electron emission microscope (PEEM) [141-143], and full field transmission soft and hard X-ray microscopes. A recent (mini)review by de Groot et al. [139] summarizes and compares these and electron-based methods for space-resolved structure determination and illustrates the sample requirements. Resolution in the 10 nm domain have been reached using soft X-rays [144,145]. Hard X-rays are more difficult to diffract [146], limiting the space resolution currently to a few tens of nm at best [147]. PEEM reaches nm-size resolution [143,148], but because it is electron-based, in situ measurements are more complex.

An early example of measuring a functioning catalyst using STXM illustrates a successful marriage between electron microscopy and X-ray spectroscopy. An environmental cell, designed for the electron microscope found successful application at the synchrotron. The structure of the Fischer-Tropsch synthesis catalyst was determined at the tens of nm length scale [149,150]. The Fischer–Tropsch reaction enables the production of high-purity chemicals and transportation fuels from sources other than conventional crude oil, most notably natural gas, coal and biomass. The catalyst of choice is iron or cobalt based. The in situ STXM experiment first tracked the reduction of supported iron oxide particles upon heating to 350 °C in di-hydrogen (1 bar) and, subsequently, the working catalyst during the Fisher-Tropsch reaction at 250 °C in syngas. The carbon 1s XAS (284 eV), oxygen 1s XAS (543 eV) and iron 2p XAS (707 eV) were measured each 35x35 nm^2 pixel. The Fe 2p XAS was used to map the iron valence and the oxygen K edge to distinguish between different oxygen-containing species (Figure 11). The extent and rate of reduction of the iron oxide phase depended on its chemical surroundings and the extent of interaction with the underlying support material. Up to 400 °C very inhomogeneous reduction occurred with metallic regions co-existing with oxide regions. Above 400 °C, the distribution of iron over the particle became more and more homogeneous and no regions were observed where iron metal was the main contributing species. Not illustrated here, it was shown that at least two

types of carbon deposits formed. Their structure depended on the location of formation at the iron nanoparticles and away from the iron nanoparticles [149,150].

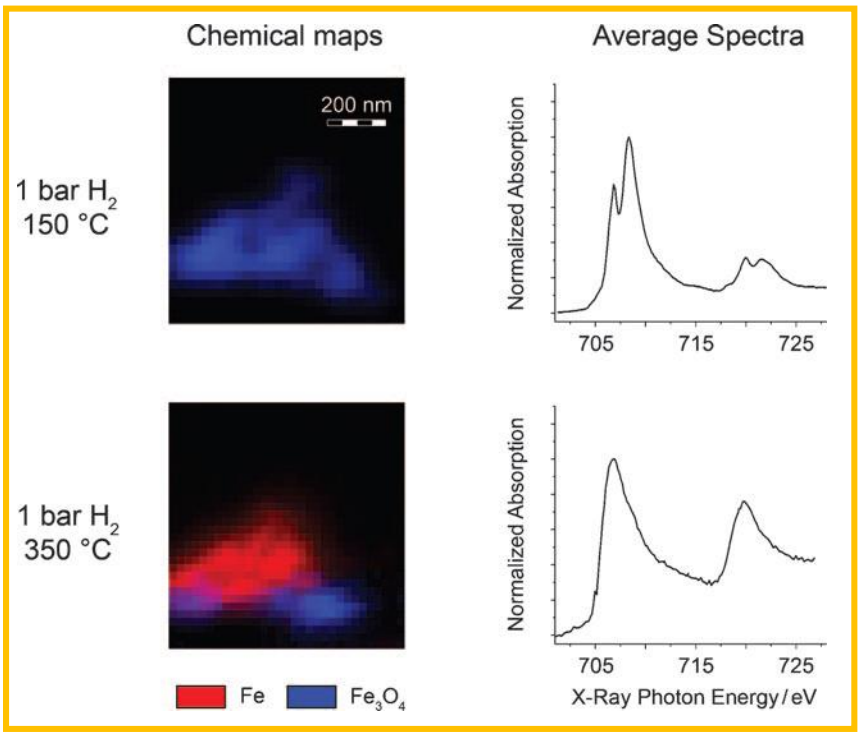

Figure 11. Structure – location relation of iron species in the Fischer-Tropsch catalyst. Left panels: chemical maps of Fe^0 and Fe_3O_4 over an iron catalyst particle at 150 °C (top) and 350 °C (bottom). The valence contours identify the variation of valence within a single particle. Each pixel measures 35x35 nm^2. Right side: Fe $L_{2,3}$ edge spectra averaged over the entire particle at the indicated conditions. Figure reproduced with permission from Ref. [149] copyright Nature Publishing Group. 2008.

These results illustrate that bulk experiments provide insufficient detail to extrapolate to the nanoscale. However, the reverse is also true. As is the case for any microscopic method, one observes only a tiny fraction of the sample. It has to be assured that what is measured is a relevant representation of the part of the sample that is responsible for its function, in our case catalytic conversion.

5 Emerging methods

5.1 X-ray emission spectroscopy

X-ray absorption spectroscopy is well-established and applied in catalysis since many decades. More recently X-ray emission has emerged as valuable and often-used tool yielding

complementary information. HERFD, XES, rXES, RIXS, and HEROS [51,151-156] are all being explored and applied to solve questions related to catalyst structure [36,91,157-166]. See chapter 6 of this book by Glatzel et al. [8]. These photon-in photon-out techniques can, like XAS, be applied under actual catalytic conditions and the most recent developments aim to increase their time resolution. The first application of some of these methods involved catalysts and were executed under in situ conditions.

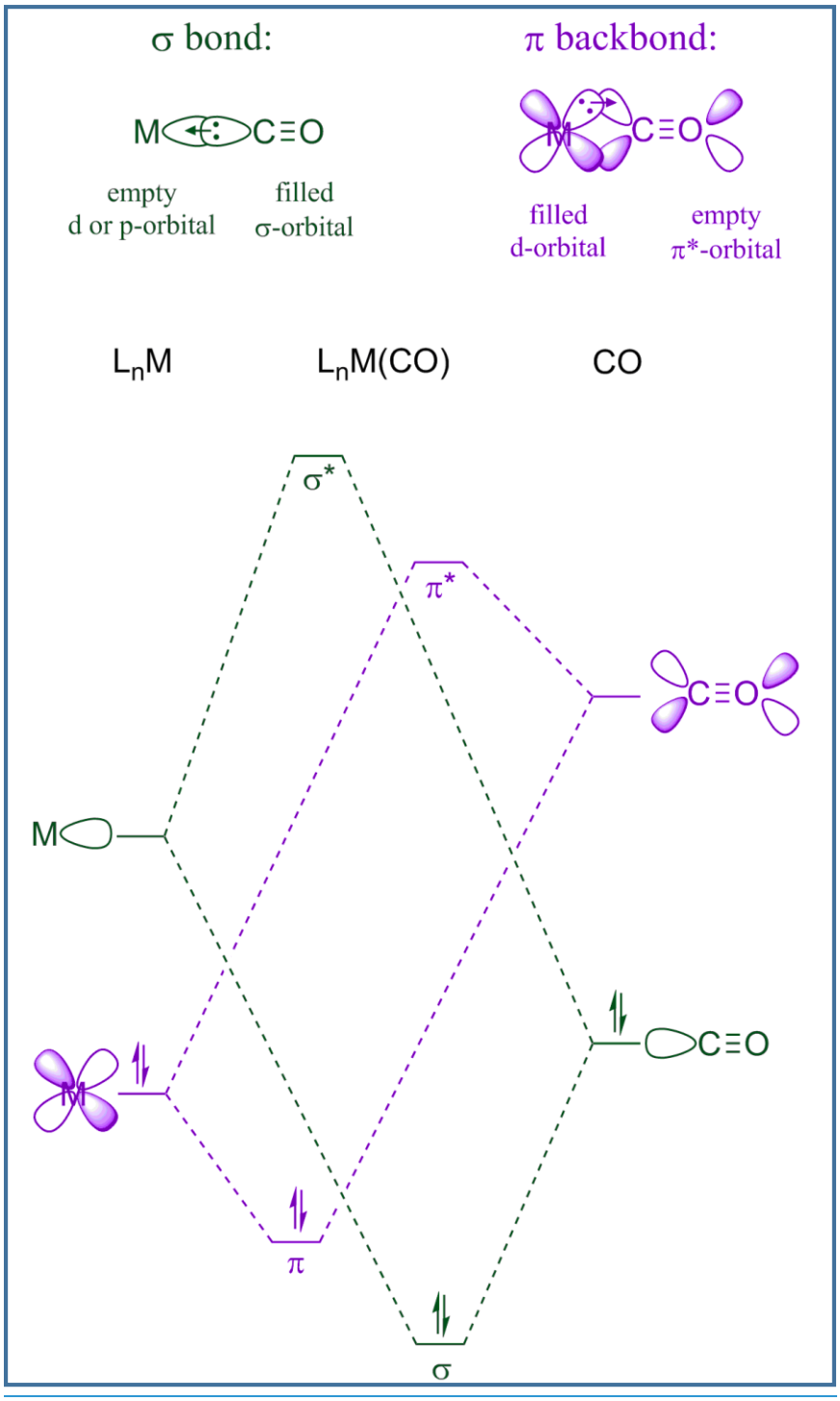

Figure 12. Bonding scheme of CO on the surface of a metal: there is σ bonding and π back-bonding resulting in charge transfer to and from the metal respectively. Unpublished figure.

An early example of the application of HERFD in the field of catalysis is that of CO chemisorption on the surface of platinum nano-particles [167]. CO can be a reactant, for example

in reactions that occur in the car exhaust (oxidation to CO_2) and during preferential oxidation of CO (PROX) to remove CO from hydrogen for use in fuel cell. Because of its strong bonding, it can also be a catalyst poison, which is well-known in fuel cells, which must operate at CO concentrations below about 10 ppm. The bonding of CO on metal surfaces is described by the Dewar–Chatt–Duncanson or Blyholder model. The 5σ molecular orbital of the CO donates electron density to a metal d orbital via σ overlap. The metal donates electrons back (the back-bonding) to the CO by overlap between a (filled) d orbital and the 2π* CO anti-bonding orbital via π overlap (Figure 12) [168,169].

Pt L_3 edge XANES probes empty d density of states and is thus sensitive to the bonding of adsorbates on the surface of metals according to the model described above. In general, surface adsorption on nano-sized particles causes strong changes in the absorption near edges. The so-called delta-mu technique as developed by Ramaker and Koningsberger has provided spectral signatures of difference spectra between a particle with adsorbate and without, yielding the adsorption mode of reactant and intermediate and its amount [170]. As mentioned above, during CO oxidation under oxygen lean conditions, the surface is poisoned by CO. CO desorption must occur before oxygen can dissociatively adsorb. L_3 edge HERFD, detected by measuring the Pt $L_{\alpha 1}$ (9442 eV) fluorescence line and normal XAS spectra of platinum nano-sized particles before and after adsorption of CO showed large spectral differences (Figure 13) [167]. The high energy-resolution of the HERFD experiment identified clear spectral features that enabled assigning of the adsorption site of CO on the nano-sized particle. Adsorption of CO on platinum occurs by σ-bonding and π-back-bonding, as shown in Figure 12. The latter forms anti-bonding d density of states that is clearly probed in the HERFD experiment in the whiteline that is split into a doublet. Theoretical simulations using the FEFF-code [171] enabled identification of the adsorption site, which was the atop site. HERFD and classical XAS probe the unfilled density of states, thus all states above the Fermi level. Measuring valence to core (VtC) emission spectroscopy in an energy-dispersive manner provides the density of states of the valence electrons [36,153,157]. Thus the combination of XAS and XES enables detecting both the bonding and anti-bonding orbitals and provide the bonding interactions on the metal. VtC XES and RIXS at the Pt L_3 edge has been measured on CO adsorbed on the platinum nano-particles of the example above [161].

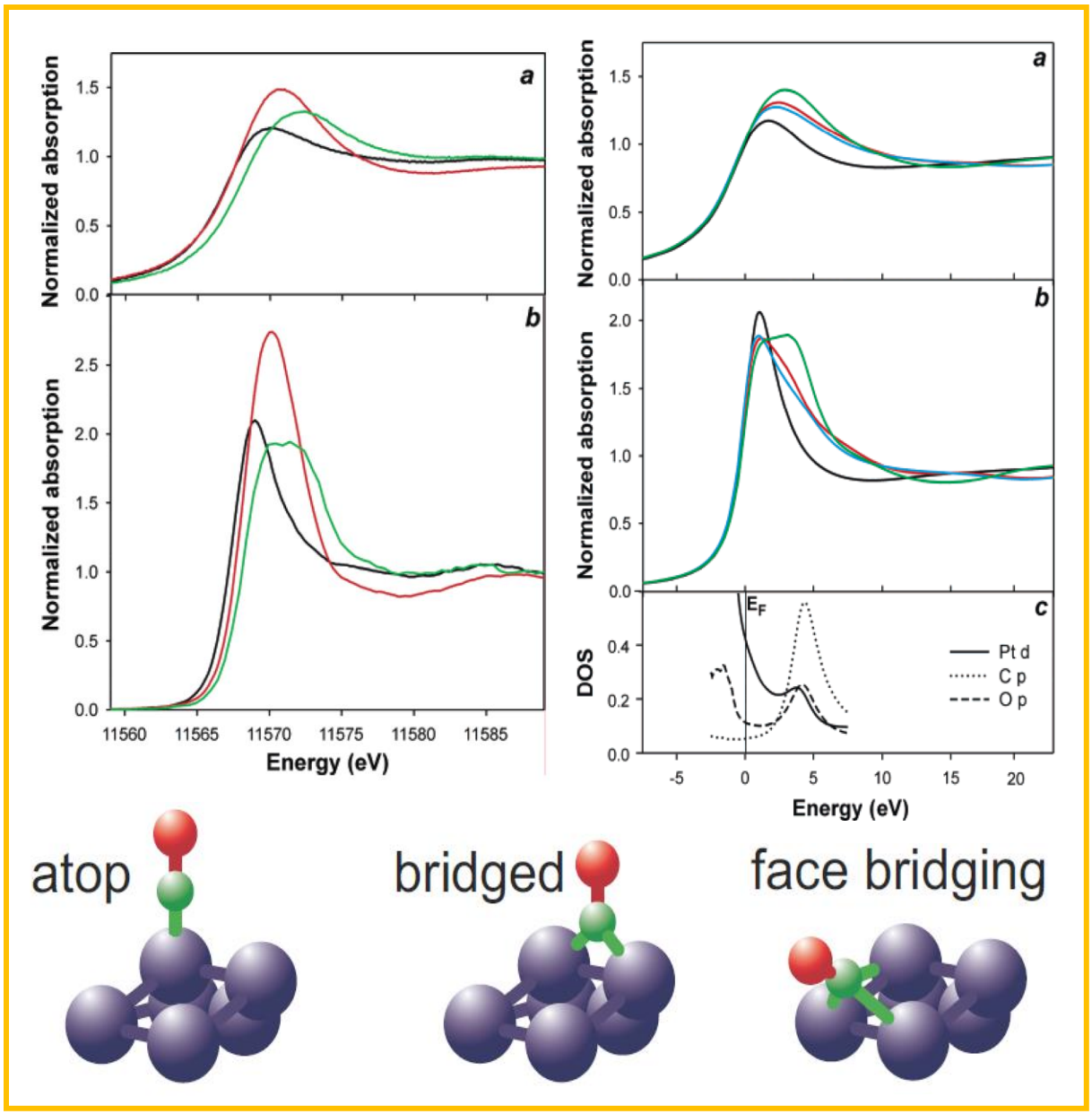

Figure 13. Experimental (left) Pt L_3 XANES (a) and HERFD XAS obtained from a horizontal plane Rowland circle spectrometer tuned to the Pt $L_{\alpha 1}$ (9442 eV) fluorescence line using the (660) Bragg reflection of one spherically bent Ge wafer; (b) of supported platinum nano-particles free of adsorbates (black), with CO (green) and covered with surface oxide (red). The right panel shows the theoretically reproduced XANES (a) and HERFD XAS (b) spectra of CO adsorbed on an atop site (green), on a bridge site (red), and on a face bridging, threefold site (blue). C shows the Pt d and C and O p densities of states, identifying overlap between platinum d and C and O p orbitals. At the bottom, the three possible adsorption modes of CO on the platinum particles is given. Theory predicts the CO to be adsorbed on atop sites. Figure reproduced with permission from Ref. [167], copyright ACS, 2006.

Figure 14 illustrates the transitions that are involved in the rRIXS experiment. A Pt 2p electron is excited by a photon of energy Ω into the 5d level. This excitation probes the XAS spectrum. Emission of a photon with energy ω leads to decay of the intermediary state, leading to deposition of energy (Ω-ω) into the sample, the so-called energy transfer, which is the equivalent of a charge-neutral excitation within the 5d levels. These transitions are the same as probed in a UV-Vis experiment, however with different transition probabilities. The lifetime τ of the 2p core hole broadens the spectrum along the incident energy direction but not along the energy transfer axis [153].

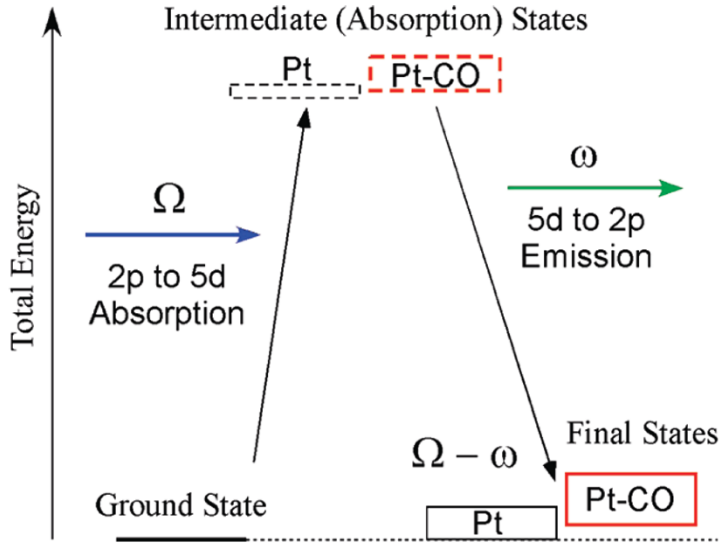

Figure 14. XAS and XES transitions in a RIXS experiment. 2p to 5d absorption (Ω) yields the intermediate state that by 5d to 2p emission (ω) produces the final state. The transition is the equivalent of a charge-neutral inter d-band excitation. The energy transfer is Ω - ω, which is the energy often depicted in RIXS planes. Figure reproduced with permission from Ref. [161], copyright ACS, 2006.

Figure 15 shows the experimental RIXS planes of platinum nano-particles after reduction and hydrogen removal and after adsorption of CO. The bands in the RIXS planes arise from valence-band (d-d) excitations, which are forbidden in UV-vis, but allowed in the RIXS experiment, because of the two-photon process. The bare particle shows the Fermi level crossing the platinum 5d band, visible by the merging of the elastic peak at zero energy transfer and valence band excitations. Theoretical simulation of the RIXS planes shows the best agreement of

experimental spectrum with atop-adsorbed CO, like the Pt L_3 HERFD in Figure 13. After CO adsorption, a band gap appears in the experimental RIXS plane, very similar to the theoretically calculated one of atop-adsorbed CO.

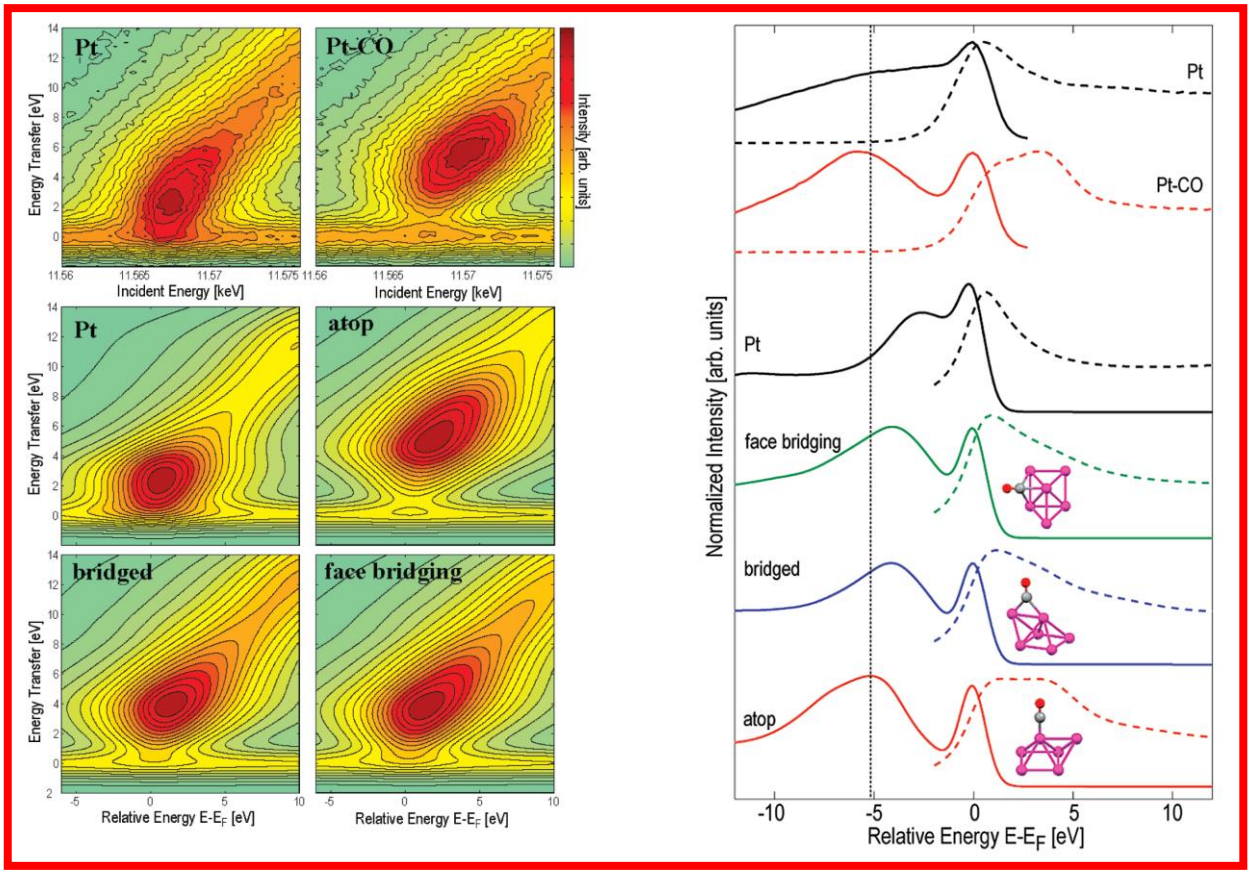

Figure 15. Pt $2p_{3/2}$ RIXS planes, experimental (top left, Pt and Pt-CO) on nano-sized platinum particles on support in the absence respectively presence of adsorbed CO. CO adsorption causes an increase in the transfer energy, which is indicative of a stabilization of the d band, lowering it in energy. Left bottom four panels: Theoretical simulations on CO adsorbed on platinum in different adsorption sites identified the CO to be adsorbed in the atop site. Right panel: Extracted XAS and XES from the planes at the left; top two are the experimental data. . Figure reproduced with permission from Ref. [161], copyright ACS, 2006.

CO adsorption modifies the electronic structure of the platinum nano-particles [172,173], which is a further example of how the simple adsorption of reactants, intermediates, and poisons affect the catalyst structure, beyond occupying a reactive site. In addition to these changes in electronic structure, CO adsorption, like that of hydrogen, induces lengthening of the Pt – Pt bond. The

accessibility of optically forbidden transitions using hard X-rays at higher resolution [163,174,175] is likely to find much wider application as more secondary emission detectors become available. The use of hard X-rays enables measuring under *in situ* and *operando* conditions fulfilling the requirement of a realistic catalysis experiment. As stated above, to determine structural changes after a change in conditions, such as temperature and gas composition or to probe the development of the catalyst over time, time-resolution is essential. The previous example of XES and RIXS was measured using a Johann type emission spectrometer, which scans the energy of the emitted radiation using spherically bent analyzer crystals, which is a time-consuming process. Using a von Hamos spectrometer [176] enables the energy dispersive detection of the emitted radiation, which enables measuring in the time domain [8,14]. Emission spectra can be obtained in a single shot and in case of limited S/N, repetition of the experiment is needed. The first examples of fast RIXS and XES are appearing [177,178]. A single pulse from a free electron laser is able to produce a measurable XES signal [179]. It is obvious to predict that these are very early developments and that these tools and methods will find much wider application in catalysis.

5.2 Pump probe methods

The above-mentioned techniques enable measuring X-ray spectroscopy at millisecond time resolution. Faster measurements can be reached using pump – probe schemes [180-187] as highlighted by the chapters of Chen [11] and Milne et al. [14] in this book. Most-often laser-excitation induces a change in the system and the response and relaxation can be detected by an X-ray probe. XAS and XES are both used and pico, nano-, and micro-second time scales are accessible. Catalytic processes that are mostly studied are those relevant to photo-catalysis [188]. Stopped-flow and stopped-flow-freeze experiments have been introduced to measure reaction mechanisms in homogeneous catalytic systems. The fast freezing of the mixture after initiating a reaction by mixing two reactant flows for example provides ample of time to measure the X-ray spectroscopy [189].

Interestingly, the general field of X-ray spectroscopy on catalysis is dominated by heterogeneous samples, pump – probe schemes are often executed on liquid systems. This originates most probably from the need to refresh samples for repeated measurement, which is simplified in a liquid jet.

6 Conclusion and outlook

X-ray spectroscopy has contributed significantly to the understanding of how heterogeneous catalysts function, because it enables determining detailed geometric and electronic structures of non-crystalline matter in an element-specific manner, measuring under exact catalytic conditions, and reaching high time and space resolutions. Methods continue to be developed rapidly yielding more detailed information. Time resolution at the scale of catalyst pre-treatment has been accessible for decades, however the achievable time resolution at the macro-kinetic time scale of reactions has enabled to identify the actual structure of the reacting species in the catalyst. Building on developments in other spectroscopies, modulated excitation and the concurrent detection of the minority species that are the active sites is introduced and transient measurements identify what are the relevant structural changes in the catalyst that govern the catalytic reaction. In the future, we expect that identification of the ensemble of atoms that contribute to catalytic reactivity, which one may call the catalytically active site, will find much wider interest. The time-resolved methods and needed instrumentation are available and continue to be developed and improved.

Space- and time-resolved measurements in a plug-flow reactor yields the complete and often changing catalyst structure. Such data and those revealing the catalytically active site will have to be integrated with macro-kinetic measurements. Essential ingredient of unravelling the active site and its role in a reaction is the understanding of the reaction mechanism. We encourage better integration of these historically separated fields. This expands to the application of complementary techniques, such as infrared, Raman and NMR spectroscopies and X-ray scattering methods to probe complementary information and notably, the time-dependent structure of reaction intermediates. Various illustrative examples of simultaneous measuring have appeared and reviewed in this book in the last part of chapter 11 by Fernández García et al. [12] and we encourage these developments. It is important to keep in mind if such measurement is to be performed at the same time on the same sample. This highly complicates the set-up and the measurements and runs the risk of obtaining sub-optimal information from any of the methods. Especially the addition of vibrational spectroscopies, like Raman and infrared, is attractive as they provide complementary data about reaction intermediates.

Given the rapid development of time- and space-resolved XAS and XES, the increased integration of existing tools from other fields, such as in situ cells from environmental EM and modulated excitation and analysis, and the creation of permanent instrumentation at multiple beam lines optimized for performing in situ measurements focused on catalysis, XAS and XES on catalysts will continue to develop rapidly. Given their time-structure in the femto-second regime, X-ray free-electron lasers [14] will play an essential role in understanding fundamental and individual reaction steps. Observing a single (sub)nano-meter-sized particle performing a catalytic reaction [49] and recording the real-time catalytic reaction at a surface remain dreams that we expect to be fulfilled within the next decade.

References

[1] G. Ertl, H. Knözinger, F. Schuth, and J. Weitkamp, *Handbook of Heterogeneous Catalysis*, John Wiley & Sons, Weinheim, 1999-2014.

[2] S. Bordiga, E. Groppo, G. Agostini, J.A. van Bokhoven, and C. Lamberti, Reactivity of Surface Species in Heterogeneous Catalysts Probed by In Situ X-ray Absorption Techniques, *Chem. Rev.*, **113**, 1736-1850 (2013).

[3] F. Bonino, E. Groppo, C. Prestipino, G. Agostini, A. Piovano, D. Gianolio, L. Mino, E. Gallo, and C. Lamberti, Catalyst Characterization by XAS and XES Spectroscopies: In Situ and Operando Experiments, *in Synchrotron Radiation*, Settimio Mobilio, Federico Boscherini, and Carlo Meneghini (Eds), Vol. Springer Berlin Heidelberg, 2014, pp. 717-736.

[4] M.A. Newton, A.J. Dent, and J. Evans, Bringing time resolution to EXAFS: recent developments and application to chemical systems, *Chem. Soc. Rev.*, **31**, 83-95 (2002).

[5] M.A. Newton, Dynamic adsorbate/reaction induced structural change of supported metal nanoparticles: heterogeneous catalysis and beyond, *Chem. Soc. Rev.*, **37**, 2644-2657 (2008).

[6] J.D. Grunwaldt, B. Kimmerle, A. Baiker, P. Boye, C.G. Schroer, P. Glatzel, C.N. Borca, and F. Beckmann, Catalysts at work: From integral to spatially resolved X-ray absorption spectroscopy, *Catalysis Today*, **145**, 267-278 (2009).

[7] J.D. Grunwaldt and C.G. Schroer, Hard and soft X-ray microscopy and tomography in catalysis: bridging the different time and length scales, *Chem. Soc. Rev.*, **39**, 4741-4753 (2010).

[8] P. Glatzel, R. Alonso-Mori, and D. Sokaras, Hard X-ray Photon-in/Photon-out spectroscopy: instrumentation, theory and applications, *in XAS and XES; Theory and Applications*, Jeroen A. van Bokhoven and Carlo Lamberti (Eds), Vol. 1, John Wiley & Sons, 2015.

[9] M. Nachtegaal, O. Müller, C. König, and R. Frahm, QEXAFS: Techniques and scientific applications for time resolved XAS, *in XAS and XES; Theory and Applications*, Jeroen A. van Bokhoven and Carlo Lamberti (Eds), Vol. 1, John Wiley & Sons, 2015.

[10] O. Mathon, I. Kantor, and S. Pascarelli, Time-resolved XAS using an energy dispersive spectrometer: techniques and applications, *in XAS and XES; Theory and Applications*, Jeroen A. van Bokhoven and Carlo Lamberti (Eds), Vol. 1, John Wiley & Sons, 2015.
[11] L.X. Chen, X-ray Transient Absorption Spectroscopy, *in XAS and XES; Theory and Applications*, Jeroen A. van Bokhoven and Carlo Lamberti (Eds), Vol. 1, John Wiley & Sons, 2015.
[12] C. Lamberti, E. Borfecchia, J.A. van Bokhoven, and M. Fernández García, XAS spectroscopy: Related Techniques and Combination with other spectroscopic and scattering Methods, *in XAS and XES; Theory and Applications*, Jeroen A. van Bokhoven and Carlo Lamberti (Eds), Vol. 2, John Wiley & Sons, 2015.
[13] T. Kroll, M. Lundberg, and E.I. Solomon, X-ray Absorption and RIXS on Coordination Complexes, *in XAS and XES; Theory and Applications*, Jeroen A. van Bokhoven and Carlo Lamberti (Eds), Vol. 2, John Wiley & Sons, 2015.
[14] W. Gawelda, J. Szlachetko, and C.J. Milne, X-ray spectroscopy at Free Electron Lasers, *in XAS and XES; Theory and Applications*, Jeroen A. van Bokhoven and Carlo Lamberti (Eds), Vol. 2, John Wiley & Sons, 2015.
[15] S.R. Bare and J. Cutler, Industrial Applications, *in XAS and XES; Theory and Applications*, Jeroen A. van Bokhoven and Carlo Lamberti (Eds), Vol. 2, John Wiley & Sons, 2015.
[16] J.D. Kistler, P. Serna, K. Asakura, and B.C. Gates, Surface metal complexes and their applications, *in XAS and XES; Theory and Applications*, Jeroen A. van Bokhoven and Carlo Lamberti (Eds), Vol. 2, John Wiley & Sons, 2015.
[17] A.V. Soldatov and K.A. Lomachenko, Nanostructured materials, *in XAS and XES; Theory and Applications*, Jeroen A. van Bokhoven and Carlo Lamberti (Eds), Vol. 2, John Wiley & Sons, 2015.
[18] J.H. Sinfelt, Structure of Bimetallic Clusters, *Accounts Chem. Res.*, **20**, 134-139 (1987).
[19] R. Prins and D.C. Koningsberger, Catalysis, *in X-Ray Absorption: Principles, Applications, Techniques of EXAFS, SEXAFS and XANES*, D. C. Koningsberger and R. Prins (Eds), Chemical analysis Vol. 92, John Wiley & Sons, New York, 1988, pp. 321.
[20] H. Kuroda, T. Yokoyama, K. Asakura, and Y. Iwasawa, Temperature-Dependence of Exafs Spectra of Supported Small Metal Particles, *Faraday Discuss.*, **92**, 189-198 (1991).
[21] G.H. Via and J.H. Sinfelt, Supported bimetallic cluster catalysts, *in X-ray absorption fine structure for catalysts and surfaces*, Yasuhiro Iwasawa (Ed),

Series on Synchrotron Radiation Techniques and Applications - Vol. 2 Vol. 2, World Scientific, Singapore, 1996, pp. 147-172.
[22] M. Englisch, J.A. Lercher, and G.L. Haller, Applications of XANES to catalyst characterization: supported metal particles, *in X-ray absorption fine structure for catalysts and surfaces*, Yasuhiro Iwasawa (Ed),

Series on Synchrotron Radiation Techniques and Applications - Vol. 2 Vol. 2, World Scientific, Singapore, 1996, pp. 276-303.
[23] S. Yoshida and T. Tanaka, Applications of XANES to catalyst characterization: metal oxide catalysts, *in X-ray absorption fine structure for catalysts and surfaces*, Yasuhiro Iwasawa (Ed),

Series on Synchrotron Radiation Techniques and Applications - Vol. 2 Vol. 2, World Scientific, Singapore, 1996, pp. 304-325.

[24] T. Tanaka and S. Yoshida, Applications of XANES to catalyst characterization: others, *in X-ray absorption fine structure for catalysts and surfaces*, Yasuhiro Iwasawa (Ed), Series on Synchrotron Radiation Techniques and Applications - Vol. 2 Vol. 2, World Scientific, Singapore, 1996, pp. 326-330.

[25] J.M. Thomas and G. Sankar, The role of synchrotron-based studies in the elucidation and design of active sites in titanium-silica epoxidation catalysts, *Accounts Chem. Res.*, **34**, 571-581 (2001).

[26] M. Fernandez-Garcia, XANES analysis of catalytic systems under reaction conditions, *Catal. Rev. Sci. Engin.*, **44**, 59–121 (2002).

[27] M. Rahman, P.R. Bolton, J. Evans, A.J. Dent, I. Harvey, and S. Diaz-Moreno, Application of stopped flow techniques and energy dispersive EXAFS for investigation of the reactions of transition metal complexes in solution: Activation of nickel beta-diketonates to form homogeneous catalysts, electron transfer reactions involving iron(III) and oxidative addition to iridium(I), *Faraday Discuss.*, **122**, 211-222 (2003).

[28] F.M.F. de Groot, A. Knop-Gericke, T. Ressler, and J.A. van Bokhoven, In-situ X-ray absorption spectroscopy in catalysis: X-ray absorption near edge spectroscopy, *in In-situ Spectroscopy of Catalysts*, B. M. Weckhuysen (Ed), Vol. American Scientific Publishers, Stevenson Ranch, California, USA, 2004, pp. 107-122.

[29] J.A. van Bokhoven, T. Ressler, F.M.F. de Groot, and A. Knop-Gericke, In-situ X-Ray absorption spectroscopy in catalysis: Extended X-ray absorption fine structure spectroscopy, *in In-situ Spectroscopy of Catalysts*, B. M. Weckhuysen (Ed), Vol. American Scientific Publishers, Stevenson Ranch, California, USA, 2004, pp. 123-144.

[30] A. Knop-Gericke, F.M.F. de Groot, J.A. van Bokhoven, and T. Ressler, In-situ X-ray absorption spectroscopy in catalysis: Soft X-ray absorption methods, *in In-situ Spectroscopy of Catalysts*, B. M. Weckhuysen (Ed), Vol. American Scientific Publishers, Stevenson Ranch, California, USA, 2004, pp. 145-160.

[31] T. Ressler, J.A. van Bokhoven, A. Knop-Gericke, and F.M.F. de Groot, In-situ X-ray absorption spectroscopy in catalysis: Time-resolved X-ray absorption methods, *in In-situ Spectroscopy of Catalysts*, B. M. Weckhuysen (Ed), Vol. American Scientific Publishers, Stevenson Ranch, California, USA, 2004, pp. 161-174.

[32] A.E. Russell and A. Rose, X-ray absorption Spectroscopy of low temperature fuel cell catalysts, *Chem. Rev.*, **104**, 4613-4635 (2004).

[33] S. Bordiga, A. Damin, F. Bonino, and C. Lamberti, Single site catalyst for partial oxidation reaction: TS-1 case study, *in Surface and Interfacial Organometallic Chemistry and Catalysis*, C. Copéret and B. Chaudret (Eds), Topics Organomet. Chem. Vol. 16, Springer-Verlag GmbH, Heidelberg, 2005, pp. 37-68.

[34] S. Bordiga, F. Bonino, A. Damin, and C. Lamberti, Reactivity of Ti(IV) species hosted in TS-1 towards H_2O_2-H_2O Solutions investigated by ab initio cluster and periodic approaches combined with experimental XANES and EXAFS data: a review and new highlights, *Phys. Chem. Chem. Phys.*, **9**, 4854-4878 (2007).

[35] S.R. Bare and T. Ressler, Characterization of Catalysts in Reactive Atmospheres by X-ray Absorption Spectroscopy, *Adv. Catal.*, **52**, 339-465 (2009).

[36] J. Singh, C. Lamberti, and J.A. van Bokhoven, Advanced X-ray absorption and emission spectroscopy: in situ catalytic studies, *Chem. Soc. Rev.*, **39**, 4754-4766 (2010).

[37] S. Bordiga, F. Bonino, K.P. Lillerud, and C. Lamberti, X-ray absorption spectroscopies: useful tools to understand metallorganic frameworks structure and reactivity, *Chem. Soc. Rev.*, **39**, 4885-4927 (2010).

[38] A.M. Beale, S.D.M. Jacques, and B.M. Weckhuysen, Chemical imaging of catalytic solids with synchrotron radiation, *Chem. Soc. Rev.*, **39**, 4656-4672 (2010).

[39] A. Frenkel, Applications of Extended X-ray Absorption Fine-Structure spectroscopy to studies of bimetallic nanoparticle catalysts, *Chem. Soc. Rev.*, **41**, 7965-7965 (2012).

[40] A.I. Frenkel, S. Khalid, J.C. Hanson, and M. Nachtegaal, QEXAFS in Catalysis Research: Principles, Data Analysis, and Applications, *in In-Situ Characterization of Heterogeneous Catalysts*, Jose A. Rodriguez, Jonathan C. Hanson, and Peter J. Chupas (Eds), Vol. John Wiley & Sons, Chichester, 2013, pp. 23-47.

[41] C.G. Schroer and J.-D. Grunwaldt, Spatially Resolved X-ray Absorption Spectroscopy, *in In-situ Characterization of Heterogeneous Catalysts*, Jose A. Rodriguez, Jonathan C. Hanson, and Peter J. Chupas (Eds), Vol. John Wiley & Sons, Inc., Chichester, 2013, pp. 49-73.

[42] M.A. Newton and A.J. Dent, Energy-Dispersive EXAFS: Principles and Application in Heterogeneous Catalysis *in In-Situ Characterization of Heterogeneous Catalysts*, Jose A. Rodriguez, Jonathan C. Hanson, and Peter J. Chupas (Eds), Vol. John Wiley & Sons, Chichester, 2013, pp. 75-119.

[43] A.I. Frenkel and J.C. Hanson, Combined X-ray Diffraction and Absorption Spectroscopy in Catalysis Research: Techniques and Applications, *in In-situ Characterization of Heterogeneous Catalysts*, Jose A. Rodriguez, Jonathan C. Hanson, and Peter J. Chupas (Eds), Vol. John Wiley & Sons, Inc., Chichester, 2013, pp. 345-367.

[44] M.A. Newton and M. Fernández-García, Combining Infrared Spectroscopy with X-ray Techniques for Interrogating Heterogeneous Catalysts, *in In-situ Characterization of Heterogeneous Catalysts*, Jose A. Rodriguez, Jonathan C. Hanson, and Peter J. Chupas (Eds), Vol. John Wiley & Sons, Inc., Chichester, 2013, pp. 369-409.

[45] F. Bonino, C. Lamberti, S. Chavan, J.G. Vitillo, and S. Bordiga, CHAPTER 4 Characterization of MOFs. 1. Combined Vibrational and Electronic Spectroscopies, *in Metal Organic Frameworks as Heterogeneous Catalysts*, F. Llabrés i Xamena and J. Gascon (Eds), Vol. The Royal Society of Chemistry, 2013, pp. 76-142.

[46] E. Borfecchia, D. Gianolio, G. Agostini, S. Bordiga, and C. Lamberti, CHAPTER 5 Characterization of MOFs. 2. Long and Local Range Order Structural Determination of MOFs by Combining EXAFS and Diffraction Techniques, *in Metal Organic Frameworks as Heterogeneous Catalysts*, F. Llabrés i Xamena and J. Gascon (Eds), Vol. The Royal Society of Chemistry, 2013, pp. 143-208.

[47] S. Kaya, D. Friebel, H. Ogasawara, T. Anniyev, and A. Nilsson, Electronic structure effects in catalysis probed by X-ray and electron spectroscopy, *J. Electron Spectrosc. Relat. Phenom.*, **190**, 113-124 (2013).

[48] A.I. Frenkel, M.W. Cason, A. Elsen, U. Jung, M.W. Small, R.G. Nuzzo, F.D. Vila, J.J. Rehr, E.A. Stach, and J.C. Yang, Critical review: Effects of complex interactions on structure and dynamics of supported metal catalysts, *J. Vac. Sci. Technol. A*, **32**, 17 (2014).

[49] A.I. Frenkel and J.A. van Bokhoven, X-ray spectroscopy for chemical and energy sciences: the case of heterogeneous catalysis, *J. Synchrot. Radiat.*, **21**, 1084-1089 (2014).

[50] J.A. van Bokhoven and C. Lamberti, Structure of aluminum, iron, and other heteroatoms in zeolites by X-ray absorption spectroscopy, *Coord. Chem. Rev.*, **277**, 275-290 (2014).

[51] C. Garino, E. Borfecchia, R. Gobetto, J.A. van Bokhoven, and C. Lamberti, Determination of the electronic and structural configuration of coordination compounds by synchrotron-radiation techniques, *Coord. Chem. Rev.*, **277**, 130-186 (2014).

[52] J.D. Grunwaldt, R. Wandeler, and A. Baiker, Supercritical fluids in catalysis: Opportunities of in situ spectroscopic studies and monitoring phase behavior, *Catal. Rev.-Sci. Eng.*, **45**, 1-96 (2003).

[53] M. Bauer, HERFD-XAS and valence-to-core-XES: new tools to push the limits in research with hard X-rays?, *Phys. Chem. Chem. Phys.*, **16**, 13827-13837 (2014).

[54] G. Ertl, Surface Science and Catalysis—Studies on the Mechanism of Ammonia Synthesis: The P. H. Emmett Award Address, *Catal. Rev. Sci. Eng.*, **21**, 201-223 (1980).

[55] G. Ertl, Reactions at surfaces: From atoms to complexity (Nobel lecture), *Angew. Chem.-Int. Edit.*, **47**, 3524-3535 (2008).

[56] X.C. Su, P.S. Cremer, Y.R. Shen, and G.A. Somorjai, High-pressure CO oxidation on Pt(111) monitored with infrared-visible sum frequency generation (SFG), *J. Am. Chem. Soc.*, **119**, 3994-4000 (1997).

[57] C. Lamberti, C. Prestipino, F. Bonino, L. Capello, S. Bordiga, G. Spoto, A. Zecchina, S.D. Moreno, B. Cremaschi, M. Garilli, A. Marsella, D. Carmello, S. Vidotto, and G. Leofanti, The chemistry of the oxychlorination catalyst: an in situ, time-resolved XANES study, *Angew. Chem. Int. Edit.*, **41**, 2341-2344 (2002).

[58] N.B. Muddada, U. Olsbye, L. Caccialupi, F. Cavani, G. Leofanti, D. Gianolio, S. Bordiga, and C. Lamberti, Influence of additives in defining the active phase of the ethylene oxychlorination catalyst, *Phys. Chem. Chem. Phys.*, **12**, 5605-5618 (2010).

[59] B.M. Weckhuysen, Determining the active site in a catalytic process: Operando spectroscopy is more than a buzzword, *Phys. Chem. Chem. Phys.*, **5**, 4351-4360 (2003).

[60] F.C. Meunier, The design and testing of kinetically-appropriate operando spectroscopic cells for investigating heterogeneous catalytic reactions, *Chem. Soc. Rev.*, **39**, 4602-4614 (2010).

[61] C. Lamberti, E. Groppo, G. Spoto, S. Bordiga, and A. Zecchina, Infrared Spectroscopy of Transient Surface Species, *Adv. Catal.*, **51**, 1-74 (2007).

[62] A.V. Soldatov, S. Dellalonga, and A. Bianconi, Relevant role of hydrogen-atoms in the XANES of Pd hydride, evidence of hydrogen induced unoccupied states, *Solid State Commun.*, **85**, 863-868 (1993).

[63] C. Roth, N. Benker, T. Buhrmester, M. Mazurek, M. Loster, H. Fuess, D.C. Koningsberger, and D.E. Ramaker, Determination of O H and CO coverage and adsorption sites on PtRu electrodes in an operating PEM fuel cell, *J. Am. Chem. Soc.*, **127**, 14607-14615 (2005).

[64] E. Bus and J.A. van Bokhoven, Hydrogen chemisorption on supported platinum, gold, and platinum-gold-alloy catalysts, *Phys. Chem. Chem. Phys.*, **9**, 2894-2902 (2007).

[65] D.E. Ramaker and D.C. Koningsberger, The atomic AXAFS and Delta mu XANES techniques as applied to heterogeneous catalysis and electrocatalysis, *Phys. Chem. Chem. Phys.*, **12**, 5514-5534 (2010).

[66] C. Mager-Maury, G. Bonnard, C. Chizallet, P. Sautet, and P. Raybaud, H_2-Induced Reconstruction of Supported Pt Clusters: Metal-Support Interaction versus Surface Hydride, *ChemCatChem*, **3**, 200-207 (2011).

[67] D. Scarano, S. Bordiga, C. Lamberti, G. Ricchiardi, S. Bertarione, and G. Spoto, Hydrogen adsorption and spill-over effects on H-Y and Pd-containing Y zeolites: An experimental and theoretical investigation, *Appl. Catal. A*, **307**, 3-12 (2006).

[68] M.W. Tew, J.T. Miller, and J.A. van Bokhoven, Particle Size Effect of Hydride Formation and Surface Hydrogen Adsorption of Nanosized Palladium Catalysts: L_3 Edge vs K Edge X-ray Absorption Spectroscopy, *J. Phys. Chem. C*, **113**, 15140-15147 (2009).

[69] M. Cabie, S. Giorgio, C.R. Henry, M.R. Axet, K. Philippot, and B. Chaudret, Direct Observation of the Reversible Changes of the Morphology of Pt Nanoparticles under Gas Environment, *J. Phys. Chem. C*, **114**, 2160-2163 (2010).

[70] A.L. Bugaev, A.A. Guda, K.A. Lomachenko, V.V. Srabionyan, L.A. Bugaev, A.V. Soldatov, C. Lamberti, V.P. Dmitriev, and J.A. van Bokhoven, Temperature- and Pressure-Dependent Hydrogen Concentration in Supported PdH_x Nanoparticles by Pd K-Edge X-ray Absorption Spectroscopy, *J. Phys. Chem. C*, **118**, 10416-10423 (2014).

[71] D. Teschner, J. Borsodi, A. Wootsch, Z. Revay, M. Havecker, A. Knop-Gericke, S.D. Jackson, and R. Schlogl, The roles of subsurface carbon and hydrogen in palladium-catalyzed alkyne hydrogenation, *Science*, **320**, 86-89 (2008).

[72] D. Teschner, Z. Revay, J. Borsodi, M. Havecker, A. Knop-Gericke, R. Schlogl, D. Milroy, S.D. Jackson, D. Torres, and P. Sautet, Understanding Palladium Hydrogenation Catalysts: When the Nature of the Reactive Molecule Controls the Nature of the Catalyst Active Phase, *Angew. Chem.-Int. Edit.*, **47**, 9274-9278 (2008).

[73] M.W. Tew, M. Janousch, T. Huthwelker, and J.A. van Bokhoven, The roles of carbide and hydride in oxide-supported palladium nanoparticles for alkyne hydrogenation, *J. Catal.*, **283**, 45-54 (2011).

[74] I. Langmuir, The constitution and fundamental properties of solids and liquids. part I. solids, *J. Am. Chem. Soc.*, **38**, 2221-2295 (1916).

[75] M. Boudart, Turnover rates in heterogeneous catalysis, *Chem. Rev.*, **95**, 661-666 (1995).

[76] M.S. Chen, Y.P. Zheng, and H.L. Wan, Kinetics and Active Surfaces for CO Oxidation on Pt-Group Metals Under Oxygen Rich Conditions, *Top. Catal.*, **56**, 1299-1313 (2013).

[77] J.D. Grunwaldt, S. Hannemann, C.G. Schroer, and A. Baiker, 2D-mapping of the catalyst structure inside a catalytic microreactor at work: Partial oxidation of methane over Rh/Al2O3, *J. Phys. Chem. B*, **110**, 8674-8680 (2006).

[78] J. Singh, M. Nachtegaal, E.M.C. Alayon, J. Stotzel, and J.A. van Bokhoven, Dynamic Structure Changes of a Heterogeneous Catalyst within a Reactor: Oscillations in CO Oxidation over a Supported Platinum Catalyst, *ChemCatChem*, **2**, 653-657 (2010).

[79] B. Kimmerle, J.D. Grunwaldt, A. Baiker, P. Glatzel, P. Boye, S. Stephan, and C.G. Schroer, Visualizing a Catalyst at Work during the Ignition of the Catalytic Partial Oxidation of Methane, *J. Phys. Chem. C*, **113**, 3037-3040 (2009).

[80] J. Singh, E.M.C. Alayon, M. Tromp, O.V. Safonova, P. Glatzel, M. Nachtegaal, R. Frahm, and J.A. van Bokhoven, Generating Highly Active Partially Oxidized Platinum during Oxidation of Carbon Monoxide over Pt/Al_2O_3: In Situ, Time-Resolved, and High-Energy-Resolution X-Ray Absorption Spectroscopy, *Angew. Chem.-Int. Edit.*, **47**, 9260-9264 (2008).

[81] E.M.C. Alayon, J. Singh, M. Nachtegaal, M. Harfouche, and J.A. van Bokhoven, On highly active partially oxidized platinum in carbon monoxide oxidation over supported platinum catalysts, *J. Catal.*, **263**, 228-238 (2009).

[82] P.M. Abdala, O.V. Safonova, G. Wiker, W. van Beek, H. Emerich, J.A. van Bokhoven, J. Sa, J. Szlachetko, and M. Nachtegaal, Scientific Opportunities for Heterogeneous Catalysis Research at the SuperXAS and SNBL Beam Lines, *Chimia*, **66**, 699-705 (2012).

[83] S.K. Matam, M.H. Aguirre, A. Weidenkaff, and D. Ferri, Revisiting the Problem of Active Sites for Methane Combustion on Pd/Al_2O_3 by Operando XANES in a Lab-Scale Fixed-Bed Reactor, *J. Phys. Chem. C*, **114**, 9439-9443 (2010).

[84] M. Shekhar, J. Wang, W.S. Lee, W.D. Williams, S.M. Kim, E.A. Stach, J.T. Miller, W.N. Delgass, and F.H. Ribeiro, Size and Support Effects for the Water-Gas Shift Catalysis over Gold Nanoparticles Supported on Model Al_2O_3 and TiO_2, *J. Am. Chem. Soc.*, **134**, 4700-4708 (2012).

[85] E. Groppo, C. Lamberti, S. Bordiga, G. Spoto, and A. Zecchina, The structure of active centers and the ethylene polymerization mechanism on the Cr/SiO2 catalyst: A frontier for the characterization methods, *Chem. Rev.*, **105**, 115-183 (2005).

[86] E. Groppo, C. Prestipino, F. Cesano, F. Bonino, S. Bordiga, C. Lamberti, P.C. Thune, J.W. Niemantsverdriet, and A. Zecchina, In situ, CrK-edge XAS study on the Phillips catalyst: activation and ethylene polymerization, *J. Catal.*, **230**, 98-108 (2005).

[87] C.N. Nenu, E. Groppo, C. Lamberti, A.M. Beale, T. Visser, A. Zecchina, and B.M. Weckhuysen, Dichloromethane as a selective modifying agent to create a family of highly reactive chromium polymerization sites, *Angew. Chem.-Int. Edit.*, **46**, 1465-1468 (2007).

[88] A. Zecchina, E. Groppo, and S. Bordiga, Selective catalysis and nanoscience: An inseperable pair, *Chem.-Eur. J.*, **13**, 2440-2460 (2007).

[89] A. Zecchina, S. Bordiga, and E. Groppo, *The Structure and Reactivity of Single and Multiple Sites on Heterogeneous and Homogeneous Catalysts: Analogies, Differences, and Challenges for Characterization Methods*, Wiley-V C H Verlag Gmbh, Weinheim, 2011.

[90] A. Zecchina and E. Groppo, Surface chromium single sites: open problems and recent advances, *Proc. R. Soc. A-Math. Phys. Eng. Sci.*, **468**, 2087-2098 (2012).

[91] K. Seenivasan, E. Gallo, A. Piovano, J.G. Vitillo, A. Sommazzi, S. Bordiga, C. Lamberti, P. Glatzel, and E. Groppo, Silica-supported Ti chloride tetrahydrofuranates, precursors of Ziegler-Natta catalysts, *Dalton Trans.*, **42**, 12706-12713 (2013).

[92] C. Barzan, D. Gianolio, E. Groppo, C. Lamberti, V. Monteil, E.A. Quadrelli, and S. Bordiga, The Effect of Hydrosilanes on the Active Sites of the Phillips Catalyst: The Secret for In Situ alpha-Olefin Generation, *Chem.-Eur. J.*, **19**, 17277-17282 (2013).

[93] G. Berlier, G. Spoto, S. Bordiga, G. Ricchiardi, P. Fisicaro, A. Zecchina, I. Rossetti, E. Selli, L. Forni, E. Giamello, and C. Lamberti, Evolution of extraframework iron species in Fe silicalite 1. Effect of Fe content, activation temperature, and interaction with redox agents, *J. Catal.*, **208**, 64-82 (2002).

[94] G. Berlier, A. Zecchina, G. Spoto, G. Ricchiardi, S. Bordiga, and C. Lamberti, The role of Al in the structure and reactivity of iron centers in Fe-ZSM-5-based catalysts: a statistically based infrared study, *J. Catal.*, **215**, 264-270 (2003).

[95] A. Zecchina, M. Rivallan, G. Berlier, C. Lamberti, and G. Ricchiardi, Structure and nuclearity of active sites in Fe-zeolites: comparison with iron sites in enzymes and homogeneous catalysts, *Phys. Chem. Chem. Phys.*, **9**, 3483-3499 (2007).

[96] J.A. Van Bokhoven, T.L. Lee, M. Drakopoulos, C. Lamberti, S. Thiess, and J. Zegenhagen, Determining the aluminium occupancy on the active T-sites in zeolites using X-ray standing waves, *Nat. Mater.*, **7**, 551-555 (2008).

[97] G. Agostini, C. Lamberti, L. Palin, M. Milanesio, N. Danilina, B. Xu, M. Janousch, and J.A. van Bokhoven, In Situ XAS and XRPD Parametric Rietveld Refinement To Understand Dealumination of Y Zeolite Catalyst, *J. Am. Chem. Soc.*, **132**, 667-678 (2010).

[98] S.T. Oyama and W. Li, Absolute determination of reaction mechanisms by in situ measurements of reaction intermediates, *Top. Catal.*, **8**, 75-80 (1999).

[99] J.J. Bravo-Suarez, K.K. Bando, J.I. Lu, M. Haruta, T. Fujitani, and S.T. Oyama, Transient technique for identification of true reaction intermediates: Hydroperoxide species in propylene epoxidation on gold/titanosilicate catalysts by X-ray absorption fine structure spectroscopy, *J. Phys. Chem. C*, **112**, 1115-1123 (2008).

[100] D. Baurecht and U.P. Fringeli, Quantitative modulated excitation Fourier transform infrared spectroscopy, *Rev. Sci. Instrum.*, **72**, 3782-3792 (2001).

[101] A. Urakawa, R. Wirz, T. Burgi, and A. Baiker, ATR-IR flow-through cell for concentration modulation excitation spectroscopy: Diffusion experiments and simulations, *J. Phys. Chem. B*, **107**, 13061-13068 (2003).

[102] T. Burgi and A. Baiker, In situ infrared spectroscopy of catalytic solid-liquid interfaces using phase-sensitive detection: Enantioselective hydrogenation of a pyrone over Pd/TiO2, *J. Phys. Chem. B*, **106**, 10649-10658 (2002).

[103] P. Haider and A. Baiker, Gold supported on Cu-Mg-Al-mixed oxides: Strong enhancement of activity in aerobic alcohol oxidation by concerted effect of copper and magnesium, *J. Catal.*, **248**, 175-187 (2007).

[104] M.M. Chen, N. Maeda, A. Baiker, and J. Huang, Molecular Insight into Pt-Catalyzed Chemoselective Hydrogenation of an Aromatic Ketone by In Situ Modulation-Excitation IR Spectroscopy, *ACS Catal.*, **2**, 2007-2013 (2012).

[105] F. Meemken, N. Maeda, K. Hungerbuhler, and A. Baiker, Platinum-Catalyzed Asymmetric Hydrogenation: Spectroscopic Evidence for an O-H-O Hydrogen-Bond Interaction between Substrate and Modifier, *Angew. Chem.-Int. Edit.*, **51**, 8212-8216 (2012).

[106] N. Maeda, F. Meemken, K. Hungerbuhler, and A. Baiker, Selectivity-Controlling Factors in Catalytic Methanol Amination Studied by Isotopically Modulated Excitation IR Spectroscopy, *ACS Catal.*, **3**, 219-223 (2013).

[107] R. Caliandro, D. Chernyshov, H. Emerich, M. Milanesio, L. Palin, A. Urakawa, W. van Beek, and D. Viterbo, Patterson selectivity by modulation-enhanced diffraction, *J. Appl. Crystallogr.*, **45**, 458-470 (2012).

[108] W. van Beek, A. Urakawa, and M. Milanesio, XRD–Raman and Modulation Excitation Spectroscopy, *in In-Situ Characterization of Heterogeneous Catalysts*, Jose A. Rodriguez, Jonathan C. Hanson, and Peter J. Chupas (Eds), Vol. John Wiley & Sons, Chichester, 2013, pp. 411-439.

[109] D. Ferri, M.A. Newton, and M. Nachtegaal, Modulation Excitation X-Ray Absorption Spectroscopy to Probe Surface Species on Heterogeneous Catalysts, *Top. Catal.*, **54**, 1070-1078 (2011).

[110] C.F.J. Konig, J.A. van Bokhoven, T.J. Schildhauer, and M. Nachtegaal, Quantitative Analysis of Modulated Excitation X-ray Absorption Spectra: Enhanced Precision of EXAFS Fitting, *J. Phys. Chem. C*, **116**, 19857-19866 (2012).

[111] C.F.J. Konig, T.J. Schildhauer, and M. Nachtegaal, Methane synthesis and sulfur removal over a Ru catalyst probed in situ with high sensitivity X-ray absorption spectroscopy, *J. Catal.*, **305**, 92-100 (2013).

[112] C.F.J. Konig, P. Schuh, T.J. Schildhauer, and M. Nachtegaal, High-Temperature Sulfur Removal from Biomass-Derived Synthesis Gas over Bifunctional Molybdenum Catalysts, *ChemCatChem*, **5**, 3700-3711 (2013).

[113] D. Ferri, M.A. Newton, M. Di Michiel, S. Yoon, G.L. Chiarello, V. Marchionni, S.K. Matam, M.H. Aguirre, A. Weidenkaff, F. Wen, and J. Gieshoff, Synchrotron high energy X-ray methods coupled to phase sensitive analysis to characterize aging of solid catalysts with enhanced sensitivity, *Phys. Chem. Chem. Phys.*, **15**, 8629-8639 (2013).

[114] Y. Lu, S. Keav, V. Marchionni, G.L. Chiarello, A. Pappacena, M. Di Michiel, M.A. Newton, A. Weidenkaff, and D. Ferri, Ageing induced improvement of methane oxidation activity of Pd/YFeO3, *Catal. Sci. Technol.*, **4**, 2919-2931 (2014).

[115] V. Marchionni, M.A. Newton, A. Kambolis, S.K. Matam, A. Weidenkaff, and D. Ferri, A modulated excitation ED-EXAFS/DRIFTS study of hydrothermal ageing of Rh/Al2O3, *Catal. Today*, **229**, 80-87 (2014).

[116] S.R. Wasserman, P.G. Allen, D.K. Shuh, J.J. Bucher, and N.M. Edelstein, EXAFS and principal component analysis: a new shell game, *J. Sync. Rad.*, **6**, 284-286 (1999).

[117] A. Piovano, G. Agostini, A.I. Frenkel, T. Bertier, C. Prestipino, M. Ceretti, W. Paulus, and C. Lamberti, Time Resolved in Situ XAFS Study of the Electrochemical Oxygen Intercalation in

$SrFeO_{2.5}$ Brownmillerite Structure: Comparison with the Homologous $SrCoO_{2.5}$ System, *J. Phys. Chem. C*, **115**, 1311-1322 (2011).

[118] W.H. Cassinelli, L. Martins, A.R. Passos, S.H. Pulcinelli, C.V. Santilli, A. Rochet, and V. Briois, Multivariate curve resolution analysis applied to time-resolved synchrotron X-ray Absorption Spectroscopy monitoring of the activation of copper alumina catalyst, *Catal. Today*, **229**, 114-122 (2014).

[119] H.S. Gandhi, K. Otto, A.G. Piken, and M. Shelef, Sulfate formation - catalyst and gas-phase composition effects in pulsators and comparison of 3-way with oxidation catalysts, *Abstracts Pap. Am. Chem. Soc.*, **172**, 36-36 (1976).

[120] M. Ozawa, M. Kimura, and A. Isogai, The application of Ce-Zr oxide solid-solution to oxygen storage promoters in automotive catalysts, *J. Alloy. Compd.*, **193**, 73-75 (1993).

[121] J. Kaspar, P. Fornasiero, and M. Graziani, Use of CeO_2-based oxides in the three-way catalysis, *Catal. Today*, **50**, 285-298 (1999).

[122] J. Kaspar, P. Fornasiero, and N. Hickey, Automotive catalytic converters: current status and some perspectives, *Catal. Today*, **77**, 419-449 (2003).

[123] E. Aneggi, M. Boaro, C. de Leitenburg, G. Dolcetti, and A. Trovarelli, Insights into the redox properties of ceria-based oxides and their implications in catalysis, *J. Alloy. Compd.*, **408**, 1096-1102 (2006).

[124] S. Rossignol, Y. Madier, and D. Duprez, Preparation of zirconia-ceria materials by soft chemistry, *Catal. Today*, **50**, 261-270 (1999).

[125] T. Yamamoto, A. Suzuki, Y. Nagai, T. Tanabe, F. Dong, Y. Inada, M. Nomura, M. Tada, and Y. Iwasawa, Origin and dynamics of oxygen storage/release in a Pt/ordered CeO_2-ZrO_2 catalyst studied by time-resolved XAFS analysis, *Angew. Chem.-Int. Edit.*, **46**, 9253-9256 (2007).

[126] O.V. Safonova, A.A. Guda, C. Paun, N. Smolentsev, P.M. Abdala, G. Smolentsev, M. Nachtegaal, J. Szlachetko, M.A. Soldatov, A.V. Soldatov, and J.A. van Bokhoven, Electronic and Geometric Structure of Ce^{3+} Forming Under Reducing Conditions in Shaped Ceria Nanoparticles Promoted by Platinum, *J. Phys. Chem. C*, **118**, 1974-1982 (2014).

[127] T. Ressler, J. Wienold, R.E. Jentoft, O. Timpe, and T. Neisius, State kinetics of the oxidation of MoO_2 investigated by time-resolved X-ray absorption spectroscopy, *Solid State Commun.*, **119**, 169-174 (2001).

[128] T. Ressler, J. Wienold, R.E. Jentoft, and T. Neisius, Bulk structural investigation of the reduction of MoO_3 with propene and the oxidation of MoO_2 with oxygen, *J. Catal.*, **210**, 67-83 (2002).

[129] T. Ressler, Solid-state kinetics and catalytic behavior of selective oxidation catalysts from time-resolved XAFS investigations, *Catal. Today*, **145**, 258-266 (2009).

[130] M.M. Bettahar, G. Costentin, L. Savary, and J.C. Lavalley, On the partial oxidation of propane and propylene on mixed metal oxide catalysts, *Appl. Catal. A-Gen.*, **145**, 1-48 (1996).

[131] P. Mars and D.W. van Krevelen, Oxidations carried out by means of vanadium oxide catalysts, *Chem. Ing. Sci.*, **3**, 41-59 (1954).

[132] B. Grzybowska, J. Haber, and J. Janas, Interaction of allyl iodide with molybdate catalysts for the selective oxidation of hydrocarbons, *J. Catal.*, **49**, 150-163 (1977).

[133] P.A. Batist, C.J. Kapteijns, B.C. Lippens, and G.C.A. Schuit, The catalytic oxidation of 1-butene over bismuth molybdate catalysts: III. The reduction of bismuth oxide, molybdenum oxide, bismuth molybdate, and of some nonstoichiometric molybdenum oxides with 1-butene, *J. Catal.*, **7**, 33-49 (1967).

[134] T. Ressler, A. Walter, Z.D. Huang, and W. Bensch, Structure and properties of a supported MoO_3-SBA-15 catalyst for selective oxidation of propene, *J. Catal.*, **254**, 170-179 (2008).

[135] M. Weber, M. Weber, and M. Kleine-Boymann, Phenol, *in Ullmann's Encyclopedia of Industrial Chemistry*, Vol. Wiley-VCH Verlag GmbH & Co. KGaA, 2004.

[136] R. Bal, M. Tada, T. Sasaki, and Y. Iwasawa, Direct phenol synthesis by selective oxidation of benzene with molecular oxygen on an interstitial-N/Re cluster/zeolite catalyst, *Angew. Chem.-Int. Edit.*, **45**, 448-452 (2006).

[137] M. Tada, Y. Uemura, R. Bal, Y. Inada, M. Nomura, and Y. Iwasawa, In situ time-resolved DXAFS for the determination of kinetics of structural changes of H-ZSM-5-supported active Re-cluster catalyst in the direct phenol synthesis from benzene and O_2, *Phys. Chem. Chem. Phys.*, **12**, 5701-5706 (2010).

[138] M. Tada, R. Bal, T. Sasaki, Y. Uemura, Y. Inada, S. Tanaka, M. Nomura, and Y. Iwasawa, Novel Re-cluster/HZSM-5 catalyst for highly selective phenol synthesis from benzene and O_2: Performance and reaction mechanism, *J. Phys. Chem. C*, **111**, 10095-10104 (2007).

[139] F.M.F. de Groot, E. de Smit, M.M. van Schooneveld, L.R. Aramburo, and B.M. Weckhuysen, In-situ Scanning Transmission X-Ray Microscopy of Catalytic Solids and Related Nanomaterials, *ChemPhysChem*, **11**, 951-962 (2010).

[140] Y. Suzuki and Y. Terada, Space-resolved XAFS, instrumentations and applications, *in XAS and XES; Theory and Applications*, Jeroen A. van Bokhoven and Carlo Lamberti (Eds), Vol. 1, John Wiley & Sons, 2015.

[141] E. Brüche, Elektronenmikroskopische Abbildung mit lichtelektrischen Elektronen, *Z. Phys.*, **86**, 448-450 (1933).

[142] J. Pohl, Formation of electron-optical images with photoelectrons, *Z. Techn. Phys.*, **15**, 579-581 (1934).

[143] G. De Stasio, L. Perfetti, B. Gilbert, O. Fauchoux, M. Capozi, P. Perfetti, G. Margaritondo, and B.P. Tonner, MEPHISTO spectromicroscope reaches 20 nm lateral resolution, *Rev. Sci. Instrum.*, **70**, 1740-1742 (1999).

[144] S. Rehbein, S. Heim, P. Guttmann, S. Werner, and G. Schneider, Ultrahigh-Resolution Soft-X-Ray Microscopy with Zone Plates in High Orders of Diffraction, *Phys. Rev. Lett.*, **103**, Art. n. 110801 (2009).

[145] W. Chao, J. Kim, S. Rekawa, P. Fischer, and E.H. Anderson, Demonstration of 12 nm Resolution Fresnel Zone Plate Lens based Soft X-ray Microscopy, *Opt. Express*, **17**, 17669-17677 (2009).

[146] G. Martinez-Criado, E. Borfecchia, L. Mino, and C. Lamberti, Micro- and Nano-X-ray Beams, *in Characterization of Semiconductor Heterostructures and Nanostructures, 2nd Edition*, C. Lamberti and G. Agostini (Eds), Vol. Elsevier Science Bv, Amsterdam, 2013, pp. 361-412.

[147] J.C. Andrews and B.M. Weckhuysen, Hard X-ray Spectroscopic Nano-Imaging of Hierarchical Functional Materials at Work, *ChemPhysChem*, **14**, 3655-3666 (2013).

[148] A. Balan, P.M. Derlet, A.F. Rodriguez, J. Bansmann, R. Yanes, U. Nowak, A. Kleibert, and F. Nolting, Direct Observation of Magnetic Metastability in Individual Iron Nanoparticles, *Phys. Rev. Lett.*, **112**, Art. n. 107201 (2014).

[149] E. de Smit, I. Swart, J.F. Creemer, G.H. Hoveling, M.K. Gilles, T. Tyliszczak, P.J. Kooyman, H.W. Zandbergen, C. Morin, B.M. Weckhuysen, and F.M.F. de Groot, Nanoscale chemical imaging of a working catalyst by scanning transmission X-ray microscopy, *Nature*, **456**, 222-U239 (2008).

[150] E. de Smit, I. Swart, J.F. Creemer, C. Karunakaran, D. Bertwistle, H.W. Zandbergen, F.M.F. de Groot, and B.M. Weckhuysen, Nanoscale Chemical Imaging of the Reduction Behavior of a Single Catalyst Particle, *Angew. Chem.-Int. Edit.*, **48**, 3632-3636 (2009).

[151] K. Hämäläinen, D.P. Siddons, J.B. Hastings, and L.E. Berman, Elimination of the Inner-Shell Lifetime Broadening in X-Ray-Absorption Spectroscopy, *Phys. Rev. Lett.*, **67**, 2850-2853 (1991).

[152] F. de Groot, High resolution X-ray emission and X-ray absorption spectroscopy, *Chem. Rev.*, **101**, 1779-1808 (2001).

[153] P. Glatzel and U. Bergmann, High resolution 1s core hole X-ray spectroscopy in 3d transition metal complexes - electronic and structural information, *Coord. Chem. Rev.*, **249**, 65-95 (2005).

[154] J. Szlachetko, M. Nachtegaal, J. Sa, J.C. Dousse, J. Hoszowska, E. Kleymenov, M. Janousch, O.V. Safonova, C. Konig, and J.A. van Bokhoven, High energy resolution off-resonant spectroscopy at sub-second time resolution: $Pt(acac)_2$ decomposition, *Chem. Commun.*, **48**, 10898-10900 (2012).

[155] L. Mino, G. Agostini, E. Borfecchia, D. Gianolio, A. Piovano, E. Gallo, and C. Lamberti, Low-dimensional systems investigated by x-ray absorption spectroscopy: a selection of 2D, 1D and 0D cases, *J. Phys. D-Appl. Phys.*, **46**, 72 (2013).

[156] P. Glatzel, T.C. Weng, K. Kvashnina, J. Swarbrick, M. Sikora, E. Gallo, N. Smolentsev, and R.A. Mori, Reflections on hard X-ray photon-in/photon-out spectroscopy for electronic structure studies, *J. Electron Spectrosc. Relat. Phenom.*, **188**, 17-25 (2013).

[157] F.M.F. de Groot, Site-selective XAFS: a new tool for catalysis research, *Topics in Catalysis*, **10**, 179-186 (2000).

[158] J.A. van Bokhoven, L. C., J.T. Miller, M. Tromp, O.V. Safonova, and P. Glatzel, Activation of oxygen on gold/alumina catalysts: In situ high-energy-resolution fluorescence and time-resolved X-ray spectroscopy, *Angew. Chem. Int. Ed.*, **45**, 4651-4654 (2006).

[159] V.A. Safonova, L.N. Vykhodtseva, Y.M. Polukarov, O.V. Safonova, G. Smolentsev, M. Sikora, S.G. Eeckhout, and P. Glatzel, Valence-to-core X-ray emission spectroscopy identification of carbide compounds in nanocrystalline Cr coatings deposited from Cr(III) electrolytes containing organic substances, *J. Phys. Chem. B*, **110**, 23192-23196 (2006).

[160] P. Glatzel, M. Sikora, G. Smolentsev, and M. Fernandez-Garcia, Hard X-ray photon-in photon-out spectroscopy, *Catalysis Today*, **145**, 294-299 (2009).

[161] P. Glatzel, J. Singh, K.O. Kvashnina, and J.A. van Bokhoven, In Situ Characterization of the 5d Density of States of Pt Nanoparticles upon Adsorption of CO, *Journal of the American Chemical Society*, **132**, 2555-2557 (2010).

[162] E. Gallo, C. Lamberti, and P. Glatzel, Investigation of the valence electronic states of Ti(IV) in Ti silicalite-1 coupling X-ray emission spectroscopy and density functional calculations, *Phys. Chem. Chem. Phys.*, **13**, 19409-19419 (2011).

[163] E. Gallo, C. Lamberti, and P. Glatzel, dd excitations in CPO-27-Ni metal-organic framework: comparison between resonant inelastic X-ray scattering and UV-vis spectroscopy, *Inorg. Chem.*, **52**, 5633-5635 (2013).

[164] E. Gallo, F. Bonino, J.C. Swarbrick, T. Petrenko, A. Piovano, S. Bordiga, D. Gianolio, E. Groppo, F. Neese, C. Lamberti, and P. Glatzel, Preference towards Five-Coordination in Ti Silicalite-1 upon Molecular Adsorption, *ChemPhysChem*, **14**, 79-83 (2013).

[165] F. Giordanino, E. Borfecchia, K.A. Lomachenko, A. Lazzarini, G. Agostini, E. Gallo, A.V. Soldatov, P. Beato, S. Bordiga, and C. Lamberti, Interaction of NH_3 with Cu-SSZ-13 Catalyst: A Complementary FTIR, XANES, and XES Study, *J. Phys. Chem. Lett.*, **5**, 1552-1559 (2014).

[166] E. Gallo, A. Piovano, C. Marini, O. Mathon, S. Pascarelli, P. Glatzel, C. Lamberti, and G. Berlier, Architecture of the Ti(IV) Sites in TiAlPO-5 Determined Using Ti K-Edge X-ray Absorption and X-ray Emission Spectroscopies, *J. Phys. Chem. C*, **118**, 11745-11751 (2014).

[167] O.V. Safonova, M. Tromp, J.A. van Bokhoven, F.M.F. de Groot, J. Evans, and P. Glatzel, Identification of CO adsorption sites in supported Pt catalysts using high-energy-resolution fluorescence detection X-ray spectroscopy, *J. Phys. Chem. B*, **110**, 16162-16164 (2006).

[168] V. Bolis, A. Barbaglia, S. Bordiga, C. Lamberti, and A. Zecchina, Heterogeneous nonclassical carbonyls stabilized in Cu(I)- and Ag(I)-ZSM-5 zeolites: Thermodynamic and spectroscopic features, *J. Phys. Chem. B*, **108**, 9970-9983 (2004).

[169] C. Lamberti, A. Zecchina, E. Groppo, and S. Bordiga, Probing the surfaces of heterogeneous catalysts by in situ IR spectroscopy, *Chem. Soc. Rev.*, **39**, 4951-5001 (2010).

[170] N. Guo, B.R. Fingland, W.D. Williams, V.F. Kispersky, J. Jelic, W.N. Delgass, F.H. Ribeiro, R.J. Meyer, and J.T. Miller, Determination of CO, H_2O and H_2 coverage by XANES and EXAFS on Pt and Au during water gas shift reaction, *Phys. Chem. Chem. Phys.*, **12**, 5678-5693 (2010).

[171] J.J. Kas, K. Jorissen, and J.J. Rehr, Real-space Multiple-scattering theory of X-ray Spectra, *in XAS and XES; Theory and Applications*, Jeroen A. van Bokhoven and Carlo Lamberti (Eds), Vol. 1, John Wiley & Sons, 2015.

[172] B. Hammer and J.K. Norskov, Why gold is the noblest of all the metals, *Nature*, **376**, 238-240 (1995).

[173] B. Hammer and J.K. Norskov, Electronic factors determining the reactivity of metal surfaces, *Surf. Sci.*, **343**, 211-220 (1995).

[174] L. Mino, V. Colombo, J.G. Vitillo, C. Lamberti, S. Bordiga, E. Gallo, P. Glatzel, A. Maspero, and S. Galli, Spectroscopic and adsorptive studies of a thermally robust pyrazolato-based PCP, *Dalton Trans.*, **41**, 4012-4019 (2012).

[175] M.M. van Schooneveld, R.W. Gosselink, T.M. Eggenhuisen, M. Al Samarai, C. Monney, K.J.J. Zhou, T. Schmitt, and F.M.F. de Groot, A Multispectroscopic Study of 3d Orbitals in Cobalt Carboxylates: The High Sensitivity of 2p3d Resonant X-ray Emission Spectroscopy to the Ligand Field, *Angew. Chem.-Int. Edit.*, **52**, 1170-1174 (2013).

[176] J. Szlachetko, M. Nachtegaal, E. de Boni, M. Willimann, O. Safonova, J. Sa, G. Smolentsev, M. Szlachetko, J.A. van Bokhoven, J.C. Dousse, J. Hoszowska, Y. Kayser, P. Jagodzinski, A. Bergamaschi, B. Schmitt, C. David, and A. Lucke, A von Hamos x-ray spectrometer based on a segmented-type diffraction crystal for single-shot x-ray emission spectroscopy and time-resolved resonant inelastic x-ray scattering studies, *Rev. Sci. Instrum.*, **83**, Art. n. 103105 (2012).

[177] J. Szlachetko, J. Sa, O.V. Safonova, G. Smolentsev, M. Szlachetko, J.A. van Bokhoven, and M. Nachtegaal, In situ hard X-ray quick RIXS to probe dynamic changes in the electronic structure of functional materials, *J. Electron Spectrosc. Relat. Phenom.*, **188**, 161-165 (2013).

[178] J. Szlachetko, D. Ferri, V. Marchionni, A. Kambolis, O.V. Safonova, C.J. Milne, O. Krocher, M. Nachtegaal, and J. Sa, Subsecond and in Situ Chemical Speciation of Pt/Al_2O_3 during Oxidation Reduction Cycles Monitored by High-Energy Resolution Off-Resonant X-ray Spectroscopy, *J. Am. Chem. Soc.*, **135**, 19071-19074 (2013).

[179] J. Szlachetko, C.J. Milne, J. Hoszowska, J.-C. Dousse, W. Błachucki, J. Sà, Y. Kayser, M. Messerschmidt, R. Abela, S. Boutet, C. David, G. Williams, M. Pajek, B.D. Patterson, G. Smolentsev, J.A. van Bokhoven, and M. Nachtegaal, Communication: The electronic structure of matter probed with a single femtosecond hard x-ray pulse, *Struct. Dynamics*, **1**, Art. n. 021101 (2014).

[180] L.X. Chen, W.J.H. Jager, G. Jennings, D.J. Gosztola, A. Munkholm, and J.P. Hessler, Capturing a photoexcited molecular structure through time-domain X-ray absorption fine structure, *Science*, **292**, 262-264 (2001).

[181] L.X. Chen, Taking snapshots of photoexcited molecules in disordered media by using pulsed synchrotron X-rays, *Angew. Chem.-Int. Edit.*, **43**, 2886-2905 (2004).

[182] C. Bressler and M. Chergui, Ultrafast X-ray Absorption Spectroscopy, *Chem. Rev.*, **104**, 1781-1812 (2004).

[183] L.X. Chen, Probing transient molecular structures in photochemical processes using laser-initiated time-resolved X-ray absorption spectroscopy, *Annu. Rev. Phys. Chem.*, **56**, 221-254 (2005).

[184] L.X. Chen and D.-J. Liu, Revealing Structural Dynamics in Catalytic Reactions Using Ultrafast Transient X-ray Absorption Spectroscopy, *Synchrotr. Rad. News*, **22**, 17-22 (2009).

[185] E. Borfecchia, C. Garino, L. Salassa, and C. Lamberti, Synchrotron ultrafast techniques for photoactive transition metal complexes, *Philos. Trans. R. Soc. A-Math. Phys. Eng. Sci.*, **371**, Art. n. 20120132 (2013).

[186] E. Borfecchia, C. Garino, L. Salassa, T. Ruiu, D. Gianolio, X.Y. Zhang, K. Attenkofer, L.X. Chen, R. Gobetto, P.J. Sadler, and C. Lamberti, X-ray transient absorption structural characterization of the (MLCT)-M-3 triplet excited state of cis- Ru(bpy)(2)(py)(2) (2+), *Dalton Trans.*, **42**, 6564-6571 (2013).

[187] M.L. Shelby, M.W. Mara, and L.X. Chen, New insight into metalloporphyrin excited state structures and axial ligand binding from X-ray transient absorption spectroscopic studies, *Coord. Chem. Rev.*, **277**, 291-299 (2014).

[188] C.J. Milne, T.J. Penfold, and M. Chergui, Recent experimental and theoretical developments in time-resolved X-ray spectroscopies, *Coord. Chem. Rev.*, **277**, 44-68 (2014).

[189] S.A. Bartlett, P.P. Wells, M. Nachtegaal, A.J. Dent, G. Cibin, G. Reid, J. Evans, and M. Tromp, Insights in the mechanism of selective olefin oligomerisation catalysis using stopped-flow freeze-quench techniques: A Mo K-edge QEXAFS study, *J. Catal.*, **284**, 247-258 (2011).